AFRL-AFOSR-UK-TR-2016-0027

Novel techniques for characterizing and understanding the response of rubbers and rubber-based composites to impact loading

Clive Siviour
THE UNIVERSITY OF OXFORD

09/30/2016
Final Report

Air Force Research Laboratory
AF Office Of Scientific Research (AFOSR)/ IOE
Arlington, Virginia 22203
Air Force Materiel Command

REPORT DOCUMENTATION PAGE

Form Approved
OMB No. 0704-0188

1. REPORT DATE *(DD-MM-YYYY)*	**2. REPORT TYPE**	**3. DATES COVERED** *(From - To)*
26-10-2016	Final	01 Mar 2012 to 28 Feb 2016

4. TITLE AND SUBTITLE
Novel techniques for characterizing and understanding the response of rubbers and rubber-based composites to impact loading

5a. CONTRACT NUMBER

5b. GRANT NUMBER
FA8655-12-1-2015

5c. PROGRAM ELEMENT NUMBER
61102F

6. AUTHOR(S)
Clive Siviour

5d. PROJECT NUMBER

5e. TASK NUMBER

5f. WORK UNIT NUMBER

7. PERFORMING ORGANIZATION NAME(S) AND ADDRESS(ES)
THE UNIVERSITY OF OXFORD
UNIVERSITY OFFICES
OXFORD, OX1 2JD GB

8. PERFORMING ORGANIZATION REPORT NUMBER

9. SPONSORING/MONITORING AGENCY NAME(S) AND ADDRESS(ES)
EOARD
Unit 4515
APO AE 09421-4515

10. SPONSOR/MONITOR'S ACRONYM(S)
AFRL/AFOSR IOE

11. SPONSOR/MONITOR'S REPORT NUMBER(S)
AFRL-AFOSR-UK-TR-2016-0027

12. DISTRIBUTION/AVAILABILITY STATEMENT
A DISTRIBUTION UNLIMITED: PB Public Release

13. SUPPLEMENTARY NOTES

14. ABSTRACT
This report describes research on the subject of rate dependence in polymers. The research explores novel techniques for characterising the high rate properties of low impedance polymers. In particular, the difficulties of testing materials with low wavespeeds are addressed using two different methods based on wave propagation:
1) Optical measurements of the evolution of displacement fields induced by stress wave propagation are used to calculate constitutive parameters using the Virtual Fields Method (VFM). In particular, different loading conditions and time-temperature superposition are explored.
2) Measurements of wave propagation in slender rods using surface mounted strain gauges allows the evaluation of complex propagation coefficients, which in turn can be used to calculate constitutive parameters of linear viscoelastic materials.

15. SUBJECT TERMS
EOARD, polymers, high rate, mechanical testing, rubber, biomaterials

16. SECURITY CLASSIFICATION OF:			**17. LIMITATION OF ABSTRACT**	**18. NUMBER OF PAGES**	**19a. NAME OF RESPONSIBLE PERSON**
a. REPORT	**b. ABSTRACT**	**c. THIS PAGE**			FOLEY, JASON
Unclassified	Unclassified	Unclassified	SAR	44	**19b. TELEPHONE NUMBER** *(Include area code)* 011-44-1895-616036

Standard Form 298 (Rev. 8/98)
Prescribed by ANSI Std. Z39.18

UNIVERSITY OF OXFORD

DEPARTMENT OF ENGINEERING SCIENCE

SOLID MECHANICS GROUP

Project USAF	**Report No.** SMG 104
Title Novel techniques for characterizing and understanding the response of rubbers and rubber-based composites to impact loading: Final Report	

SUMMARY

This report describes research on the subject of rate dependence in polymers, performed over the past four years in the project FA8655-12-1-2015: "Novel techniques for characterizing and understanding the response of rubbers and rubber-based composites to impact loading". The research presented was performed by Dr S-H Yoon and Mr Y Huang during their doctoral studies under the supervision of Dr CR Siviour.

The research explores novel techniques for characterising the high rate properties of low impedance polymers. In particular, the difficulties of testing materials with low wavespeeds are addressed using two very different methods based on wave propagation:

- Optical measurements of the evolution of displacement fields induced by stress wave propagation are used to calculate constitutive parameters using the Virtual Fields Method (VFM). In particular, different loading conditions and time-temperature superposition are explored.
- Measurements of wave propagation in slender rods using surface mounted strain gauges allows the evaluation of complex propagation coefficients, which in turn can be used to calculate constitutive parameters of linear viscoelastic materials

This report aims to provide a summary of the research performed. Further information is available in the two doctoral theses and journal publications. All publications will be made available through the Oxford University Research Archive (https://ora.ox.ac.uk/), or may be obtained from CR Siviour.

Distribution: SMG Office (1 copy + PDF) EOARD (PDF)		**Authorised by:** ACF Cocks
Date 26 September 2016	**Authors**: CR Siviour, S-H Yoon, Y Huang	**Page of pages** 1 of 42

CONTENTS

FIGURES

NOMENCLATURE

E	Young's modulus	a or $\boldsymbol{a}$	Acceleration
ρ	Density	ν	Poisson's ratio
σ or $\boldsymbol{\sigma}$	True stress	W	Strain energy
c	Elastic wavespeed	λ or $\boldsymbol{\lambda}$	Stretch ratio
v or $\boldsymbol{v}$	Particle velocity	S or $\boldsymbol{S}$	Nominal stress
ε or $\boldsymbol{\varepsilon}$	Strain	μ	Shear modulus
E^*	Complex modulus	α	Strain hardening coefficient in Ogden model or attenuation coefficient for wave propagation
E'	Storage modulus		
E''	Loss modulus	κ	Wavenumber
T or $\boldsymbol{T}$	Traction	γ	Wave propagation coefficient
$\boldsymbol{n}$	Unit normal vector	ω	Angular frequency
x or $\boldsymbol{x}$	Position	TC	Wave transmission coefficient
u or $\boldsymbol{u}$	Displacement	RC	Wave Reflection coefficient
u^* or $\boldsymbol{u^*}$	Virtual displacement		
ε^* or $\boldsymbol{\varepsilon^*}$	Virtual strain		

1 Introduction

1.1 Background and motivation

It has long been known that the mechanical properties of polymers are strong functions of temperature and frequency, and thus strain rate. Over the past 20 years, the rate dependence of a number of polymers has been characterised at strain rates from 10^{-4} to 10^{4} s^{-1}, and in some cases higher. However, there are a number of experimental challenges in high rate characterisation of polymers. The most important is that, owing to their low stress wavespeed, the structural response of the specimen can affect measurements of the intrinsic material behaviour. These challenges are particularly acute for rubbers, for which the wavespeed is typically very low, or when considering small strain properties, such as the elastic modulus, as this is during this period of the loading that dynamic effects are most prominent.

Methods for characterising the high rate response of materials, and in particular polymers, are described in a number of reviews [1-3]. One of the most common for strain rates between 500 and ~10,000 s^{-1} is the split-Hopkinson bar, in which the specimen sits between two slender rods instrumented with strain gauges. By introducing a stress wave into one of the rods, and monitoring the resulting waves using the gauges, the boundary conditions at the specimen-rod interfaces can be calculated, and the stress-strain behaviour of the specimen inferred. However, these calculations necessarily assume that the strain and stress are the same everywhere in the specimen, which is only the case if the specimen is in static equilibrium during the dynamic experiment. This is the key difficulty in applying experiments of this nature to properties of rubbers, or to small strain properties of any materials.

Furthermore, for all materials, these techniques become cumbersome for lower strain rates, where longer duration experiments are required in order to achieve large strains: this is a particularly relevant concern for elastomers, for which large strain response is often required (see Yoon thesis section 2.1). The traditional Hopkinson bar requires the period of the lowest natural frequency of the bars to be longer than the duration of the experiment (this can be overcome at the expense of accuracy). Hence, the experimentalist now has to decide whether to increase the length of their Hopkinson bar, or to move to a short load cell whose lowest natural frequency is higher than all the frequencies present in the loading. Neither of these is simple for strain rates of order 10 to 1000 s^{-1}.

A final limitation of the Hopkinson bar approach is that for viscoelastic materials the experiment samples a convolution of the viscoelastic behaviour over a range of timescales. It is not, therefore, straightforward to relate the data obtained to frequency dependence in polymers, especially because the strain rate experienced is less well controlled than in a quasi-static experiment with closed loop control.

1.2 Project summary and highlights

In this project, we designed experimental techniques and analysis to provide data on the constitutive behaviour of polymers from loading configurations in which the polymer is never in static equilibrium: the wave propagation was made an integral part of the experiment, rather than something to be avoided. In one case, optical measurements of surface strains in thin specimens were used, in the second, strain gauge measurements of strains in slender rods. For both techniques, rigorous analytical analysis was combined with Finite Element modelling to ensure that, in principle, the experimental configuration was able to give the required data, and that the data reduction techniques were correctly implemented, before applying these same techniques identically to experimental data. Addressing each of the two methods:

1.2.1 High strain rate behaviour of rubbers using the Virtual Fields Method

The recently developed Dynamic Virtual Fields Method (VFM) was identified as an appropriate technique for identifying constitutive parameters from experimental data. In particular, a version of the VFM in which measurements of external tractions are not required, and force (or stress) information is provided by measurements of accelerations in the specimen: i.e. from inertial forces arising from the passage of stress waves (see Yoon thesis chapter 3, section 2.1, references [4-8]). This is particularly suited to elastomers, since the ratio of Young's modulus to density E / ρ) is small relative to many other materials. Initially, a simple tensile experiment was developed and applied to representative elastomers. One weakness of stress-wave driven experiments is that the strain rate cannot be controlled independently of the stress, since both result from the same particle velocity fields in the specimen (in an elastic material, stress $\sigma = \rho c v$ whilst strain $\varepsilon = v/c$, where v is the particle speed induced by the wave and c is the wavespeed). Hence, in order to obtain the large amplitude data required for hyperelastic constitutive models, a technique was developed in which specimens were statically pre-stretched before the dynamic load was applied. This allowed both very large, and very small, strain data to be accurately obtained, both of which are difficult with previously existing techniques. The experiments and analysis are described in Yoon thesis chapters 4 and 5, section 2.2 of this report and paper C . Further discussion of the analysis is presented in Yoon thesis chapter 7.

A second method of achieving large strains is to allow the stress wave to reverberate in a specimen clamped at both ends: ensuring that it remains tensile after each reflection. This requires the loading to be continuous, which was achieved in this project by using an inertial system driven by a gas gun. Higher strain rates could be achieved, and a single experiment allowed the identification of parameters of a hyperelastic model; in particular, large enough strains were achieved to identify the hardening coefficient. This method is described in Yoon thesis chapter 6, section 2.3 of this report, and paper B. A further modification to the experimental apparatus was also made, in which high speed force measurements are re-introduced.

The data from these measurements improve the quality of the parameter identification during periods of the wave oscillation in which the accelerations in the specimen are small. This is discussed in detail in paper H.

Comparison of the data obtained from these tensile experiments, and those obtained from compressive experiments on the same material are given in Yoon's thesis section 7.5.2, paper G and section 2.4.1 of the current report. In addition, some work was done on a framework for model identification from the material behaviour measurements obtained (see Yoon thesis 8.2, report 2.4.2). Finally, and most importantly, a framework was developed for identification of relaxation on sub-millisecond timescales, and for time-temperature superposition to build master curves from these data. These curves were then compared to data from well-established Dynamic Mechanical Analysis (DMA) experiments on the same materials (Yoon thesis 8.3, section 2.4.3 and paper A).

1.2.2 Frequency dependence of polymers from wave propagation parameters

The wavespeed and attenuation of stress waves in any medium are dependent on the mechanical properties of the medium, including the frequency dependence of these properties. In particular, for a slender rod, they depend on the complex modulus E^*. In this research, surface mounted strain gauges were used to monitor the propagation of stress waves in slender (c.a. 1 m long, 12.7 mm diameter) rods made from a Titanium alloy and PMMA, and at interfaces between these rods. Firstly, in single rods, by taking ratios of Fourier transforms of short duration stress pulses that have propagated different distances, it is possible to extract the wavenumber and attenuation coefficients as functions of frequency. These were used to calculate the complex modulus of the material, providing accurate and repeatable measurements at frequencies from c.a. 2000 to 20,000 Hz. These methods are discussed in Huang's thesis and sections 3.1, 3.2 and 3.3 of the current report. The second technique used transmission and reflection coefficients at boundaries. Again, surface mount strain gauges were used, but this time to measure the amplitude profiles of stress pulses incident onto a boundary, and then the profiles of the resultant reflected and transmitted pulses. Fourier transforms of these pulses were again used, this time to calculate ratios and the reflection and transmission coefficients, from which the mechanical properties of one rod can be derived if those of the other are known. Extensive analytical, finite element and experimental research was performed, which is summarised in sections 3.4, 3.5 and 3.6 of the current report, and in Huang's thesis. It is anticipated that 4 papers will result from this research

1.3 Papers and other publications

This report provides a summary of the research performed. A more detailed analysis, including discussion of constitutive modelling, is available in Dr Yoon's DPhil thesis: *Application of the virtual fields method to the mechanical behaviour of rubbers under dynamic loading*, 2015, University of Oxford; and Mr Huang's thesis (pending at the time of writing). The research is also described in the following journal publications

A. S-H Yoon and CR Siviour, *"Application of the Virtual Fields Method to a relaxation behaviour of rubbers"* JMPS, *available online* doi: 10.1016/j.jmps.2016.09.001

B. S-H Yoon, M Winters and CR Siviour "*High Strain-Rate Tensile Characterization of EPDM Rubber Using Non-equilibrium Loading and the Virtual Fields Method"* Experimental Mechanics (2016) 56:25-35 doi: 10.1007/s11340-015-0068-3

C. S-H Yoon, I Giannakopoulos and CR Siviour *"Application of the Virtual Fields Method to the uniaxial behaviour of rubbers at medium strain rates"* International Journal of Solids and Structures **69-70** (2015) 553-568 doi: 10.1016/j.ijsolstr.2015.04.017

refereed conference papers

D. Y Huang and CR Siviour *"Single rod impact tests: Analytical, experimental, and modelling investigation"* EPJ Web of Conferences **94** (2015) 01052 doi: 10.1051/epjconf/20159401052

E. S-H Yoon and CR Siviour *"The dynamic Virtual Fields Method on rubbers at medium and high strain rates"* EPJ Web of Conferences **94** (2015) 01017 doi: 10.1051/epjconf/20159401017

and a non-refereed conference paper

F. S-H Yoon and CR Siviour *"The Virtual Fields Method to Rubbers Under Medium Strain Rates"* Proc.2016 SEM Annual Conference and Exposition, Orlando, Florida.

Further papers are in preparation

G. The incremental Virtual Fields Method and pre-stretching technique applied to rubbers under uniaxial medium-strain-rate loading *Submitted to Strain*

H. Application of the Virtual Fields Method to rubbers under medium strain rate deformations with using both acceleration and traction force data *Submitted to Journal of Dynamic Behavior of Materials*

I. Deriving material properties from wave propagation in slender rods *in preparation*

J. Methods for dispersion correction applied to slender rods *in preparation*

K. Wave behaviour at one dimensional interfaces part 1: Theory *in preparation*

L. Wave behaviour at one dimensional interfaces part 2: Deriving material response *in preparation*

The following conference presentations have been given (in addition to the three listed above)

S-H Yoon & CR Siviour 2014. The virtual fields method to elastomeric materials under dynamic loading. At *16th International Conference on Experimental Mechanics. Cambridge*.

S-H Yoon. and CR Siviour 2013. The virtual fields method to the uniaxial mechanical behaviour of hyperelastic materials at medium strain rate. At *21st DYMAT Technical Meeting. London*.

Y Huang, & CR Siviour 2014. Wave propagation in visco-elastic rods. At *16th International Conference on Experimental Mechanics. Cambridge*.

In addition, the research has been discussed in the following review articles

CR Siviour, JL Jordan, "*High Strain Rate Mechanics of Polymers: A Review*", J. dynamic behavior mater. (2016): 2:15-32 doi: 10.1007/s40870-016-0052-8

CR Siviour "High Strain Rate Characterization of Polymers" Proceedings of the 2015 APS Conference on Shock Compression of Condensed Matter in press

Further related activities are as follows:

CR Siviour gave the JSA *Young Investigator* lecture at the SEM Annual Conference and Exposition, 2016, on the subject of high strain rate characterisation of polymers

CR Siviour gave an invited talk at the 2015 APS Conference on Shock Compression of Condensed Matter, on the subject of high strain rate characterisation of polymers

CR Siviour and S-H Yoon took part in the Royal Society Summer Science Exhibition in 2015, on a collaborative stand with Reading University: *Materials that repair themselves*.

CR Siviour spent 3 weeks in the USA during August 2015 taking part in the Dynamic Materials and Interactions portfolio review and visiting laboratories (Eglin Air Force Base, ARL, Wright Patterson Air Force Base). This visit was funded by the Windows on Science Programme.

We are also collaborating with F Pierron at Southampton University on research related to his and our AFOSR funded programmes.

All publications will be made available through the Oxford University Research Archive (https://ora.ox.ac.uk/), or may be obtained from CR Siviour. This archive is searchable by fields including author, title and sponsor.

2 Virtual Fields Method: Methods, Assumptions, Procedures and Results

2.1 Application of the Virtual Fields Method to High Strain rate Experiments

See also Yoon thesis chapters 2 and 3

We consider a specimen, clamped at one end, and with a velocity imposed at the other end, see Figure 1. A stress wave propagates along the specimen, in front of the wave the displacement, particle velocity, and stress are zero, behind the wavefront, they are determined by the input velocity, v_0 and the material properties. Within the wavefront, there is an acceleration a_x, which is shown as constant but would usually vary with both location and time.

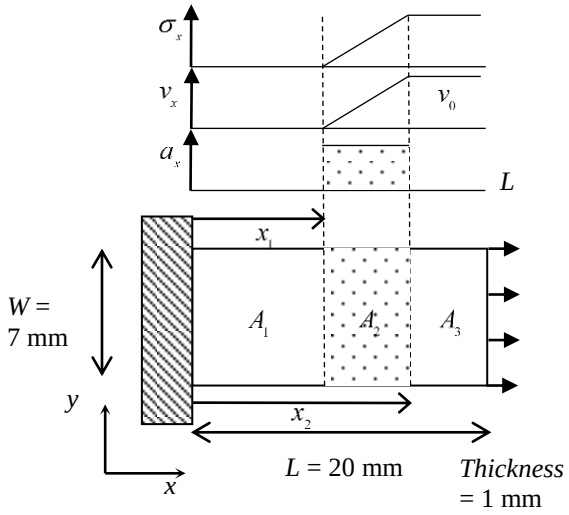

Figure 1 Axial stress, velocity and acceleration profiles as a function of position in the specimen at time t after loading and the resulting acceleration field. The acceleration is a_x in the region A_2 and zero elsewhere.

We seek to apply the Principle of Virtual Work to this specimen by writing down the dynamic equilibrium equation

$$-\int_v \boldsymbol{\sigma} : \boldsymbol{\varepsilon}^* \, \mathrm{d}v + \int_{s_f} \overline{\mathbf{T}} \cdot \boldsymbol{u}^* \, \mathrm{d}s = \int_v \rho \boldsymbol{a} \cdot \boldsymbol{u}^* \, \mathrm{d}v \qquad (1)$$

in which

$\boldsymbol{\sigma}$	*actual stress tensor*
$\overline{\mathbf{T}}$	*actual traction* $(= \boldsymbol{\sigma}\,\mathbf{n})$
$\boldsymbol{u}^*$	*virtual displacement vector*
$\boldsymbol{\varepsilon}^*$	*virtual strain tensor* $(= \partial \boldsymbol{u}^* / \partial \boldsymbol{x})$

v *current volume of the body*

s_f *current loaded surface*

‘:’ and ‘·’ *the dot products for matrices and vectors*

and then to seek a virtual displacement field $\boldsymbol{u}^*(x, y, t)$ which eliminates the surface integral containing the traction at the two ends, for example to identify the modulus, E of the specimen, we will use

$$\begin{cases} u_x^{*(1)} = x(x-L) \\ u_y^{*(1)} = 0 \end{cases} \Rightarrow \begin{cases} \varepsilon_x^{*(1)} = 2x - L \\ \varepsilon_y^{*(1)} = 0 \\ \varepsilon_{xy}^{*(1)} = 0 \end{cases} \tag{2}$$

such that

$$-\int_v \boldsymbol{\sigma} : \boldsymbol{\varepsilon}^* \, dv = \int_v \rho \boldsymbol{a} \cdot \boldsymbol{u}^* \, dv \tag{3}$$

It now remains to insert a suitable constitutive model into this equation to form a series of linear or non-linear equations, which may be solved for the constitutive parameters. In this way, it is possible to convert what is usually regarded as an inverse problem (identification of constitutive parameters from experimental data) into a forward problem, which is both conceptually easier to understand and computationally more efficient.

In practice, there are a number of constraints on experimental design. Firstly, accurate parameter identification relies on the presence of large accelerations in the specimen. Secondly, accurate displacement measurements are required at small time intervals in order to calculate accelerations and strains, although in practice the strain measurements benefit from the smoothing effect of the integrals. Such measurements can currently only be provided in dynamic experiments from high speed imaging of the specimen surface, using an appropriate subsequent image analysis technique, e.g. speckle imaging or a grid method. Hence, it is advantageous to design specimens for which these measurements are a good approximation of the internal deformation field, and in this thesis thin rectangular specimens, as indicated in Figure 1, are used. Finally, measurements must be made with a sufficient spatial resolution to convert the integrals in equation (3) to a sum over the specimen surface.

Further discussions of the application of the VFM to dynamic experiments are given in Yoon’s thesis chapters 2.3 and 3 and in [6]; discussion of errors and accuracy are given in chapter 4 and paper C; discussion of optimised virtual fields ($\boldsymbol{u}^*$) in chapters 3.3, 4.2 and 5.4.

2.2 The Linear VFM with pre-stress applied to a hyperelastic material

See also Yoon thesis chapters 4, 5 and 7 and paper C

2.2.1 Simulation results: linear elastic material with no-prestretching

A simple Finite Element (FE) simulation was performed in Abaqus explicit, simulating the geometry in figure 1. The velocity profile on the right hand side was adopted from one of the later experiments, and is shown in Figure 2 Left. Figure 2 Right shows the output displacement (u_x), strain (ε_x) and acceleration (a_x) fields, along with the virtual displacement field (u_x*) proposed in equation (2).

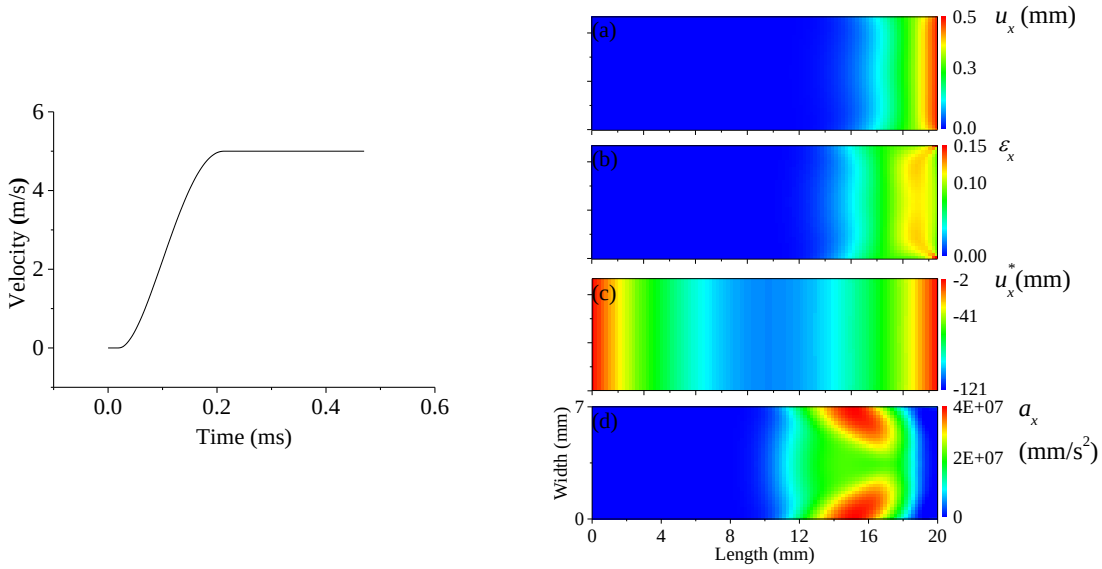

Figure 2. Left: applied velocity profile; Right (a) Axial displacement, (b) true strain, (c) virtual displacement and (d) acceleration fields of the FEM simulation of the isotropic linear elastic material at 0.2 ms.

A description of the full analysis procedure is given in Yoon's Thesis Section 4.2. Two analyses were performed, one using the displacement, strain and acceleration fields produced by the FE simulation, the second using displacement data only, and differentiating these with respect to space and time to obtain strains and accelerations respectively. The second method allows the effect of noise in the displacement data and of different high speed camera framing rates to be explored, along with the temporal smoothing required for accurate acceleration calculations. Further, simulation of specimens of different geometries were performed, showing, in particular, for the material investigated thicknesses of less than c.a. 2 mm are required. More detailed results are given in the thesis.

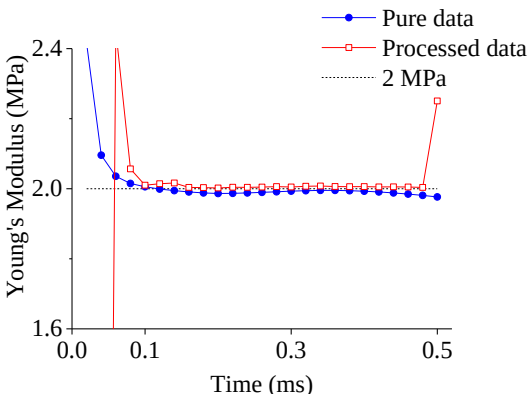

Figure 3 Young's modulus estimates from application of VFM to data from simulation of linear elastic material, $E = 2$ MPa, $\nu = 0.5$. 'Pure data' using strain and acceleration data from the FE simulation. 'Processed data, calculating these values from the displacement output.

The final output of this analysis is a series of Young's modulus estimates over time, Figure 3. It is observed that these estimates agree well with the input modulus, except at the start of the loading, during which time the area of specimen undergoing acceleration is too small for meaningful calculations.

Before moving to simulations on the hyperelastic material, it should also be noted that work was performed to optimise the virtual displacement field beyond that in equation (3) using so-called 'piecewise' virtual fields which, subject to certain constraints, can be optimised to the actual acceleration distributions in the experiments (see also Yoon's Thesis Section 3.3).

2.2.2 Simulation results: hyperelastic material with linear identification and prestretching

The aim of these experiments was to identify constitutive parameters for hyperelastic materials. A simple constitutive model which describes such materials is the Ogden model, for which the strain energy can be expressed as

$$W = \sum_{i=1}^{N} \frac{2\mu_i}{\alpha_i^2}\left(\lambda_1^{\alpha_i} + \lambda_2^{\alpha_i} + \lambda_3^{\alpha_i} - 3\right) \tag{4}$$

and the nominal stress, in the x direction for an incompressible material is

$$S_x = \sum_{i=1}^{N} \frac{2\mu_i}{\alpha_i}\left(\lambda_x^{\alpha_i - 1} - \lambda_x^{-1-0.5\alpha_i}\right) \tag{5}$$

where the λs are the principal stretch ratios, μs are shear modulus and αs strain hardening coefficients. Here, N indicates the number of terms in the model, we will mainly look at materials that can be well described by a single-term model ($N = 1$). We wish to characterise the constitutive parameters μ and α; but whilst μ can be obtained from a small-strain experiment with a linearised identification procedure (i.e. the E discussed in 2.2.1 is a measure of μ), α cannot. Instead, α was obtained, in these experiments, by statically pre-stretching the specimen, applying a small-amplitude dynamic load, calculating the stiffness apparent to that dynamic load, and then assuming that this stiffness is a tangent to the local stress-strain curve. From a series of such tangents, a simple optimisation routine was used to find μ and α. Initially, an identification procedure was developed which required a measurement of the axial force in the specimen (Yoon thesis chapter 4), but this was later updated so that only strains were required (chapter 7). The procedure is illustrated in Figure 4.

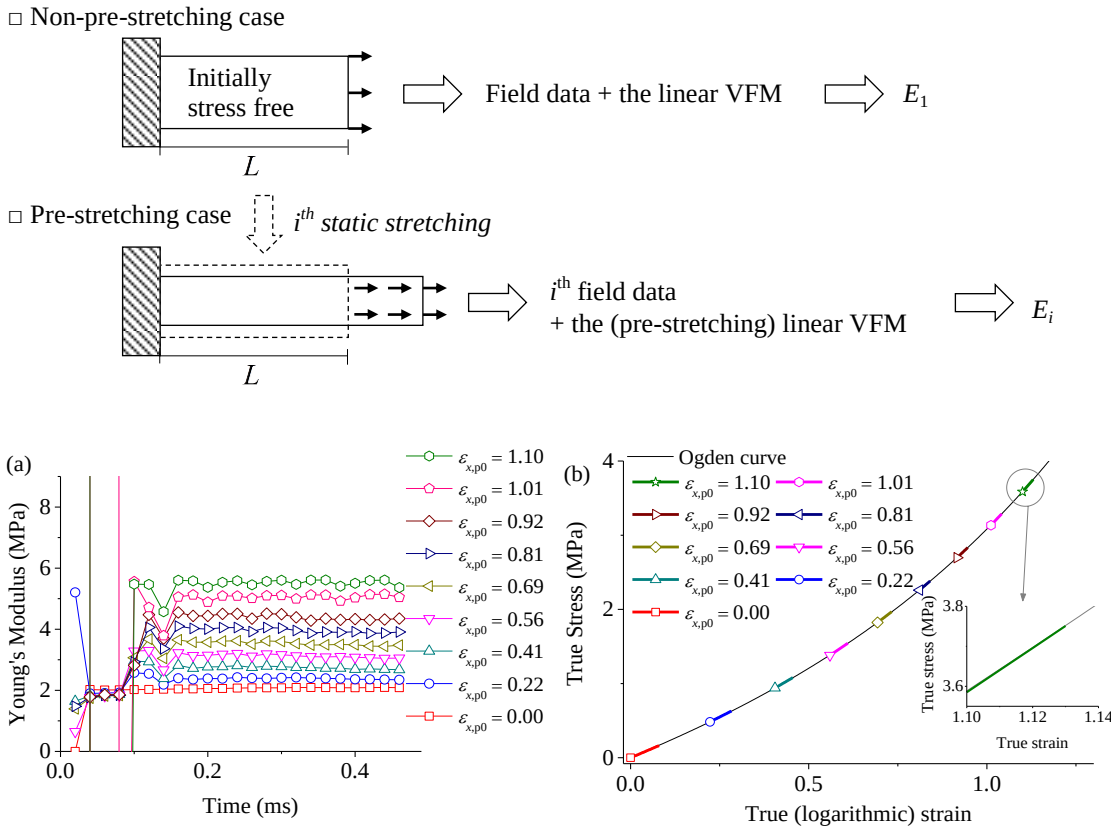

Figure 4 Procedure for identifying Ogden constitutive parameters from pre-strech expeiments. Top: An experiment may be performed in which the dynamic load is applied without pre-stretching, or the specimen may be statically stretched before being loaded dynamically. Each experiment provides a series of stiffnesses defined at each pre-strain (0.00 to 1.10, bottom left). These stiffnesses are assumed to be tangents to the stress-strain curve at each of the pre-strain locations, bottom right. The parameters μ and α are found for which the gradient of the curve best matches these tangents.

2.2.3 Experimental procedure and data

A simple dropweight system was designed which allows repeated loading of the rubber specimen, Figure 5. Images were acquired using a Phantom SA5 high speed camera; in common with all high speed cameras, the spatial resolution decreases with increasing imaging speed, making the results more susceptible to the effects of noise on the displacement measurements, whilst high speeds enable better acceleration calculations. An imaging speed of 100 kfps was found to give the best balance between these conflicting demands. A detailed study of noise is given in Yoon's Thesis Sections 5.3 and 5.4.

Figure 6 shows representative data from one of the experiments. Using a procedure identical to that applied to the simulations stiffness data are derived, and then used to calibrate the parameters of an Ogden model, Figure 7.

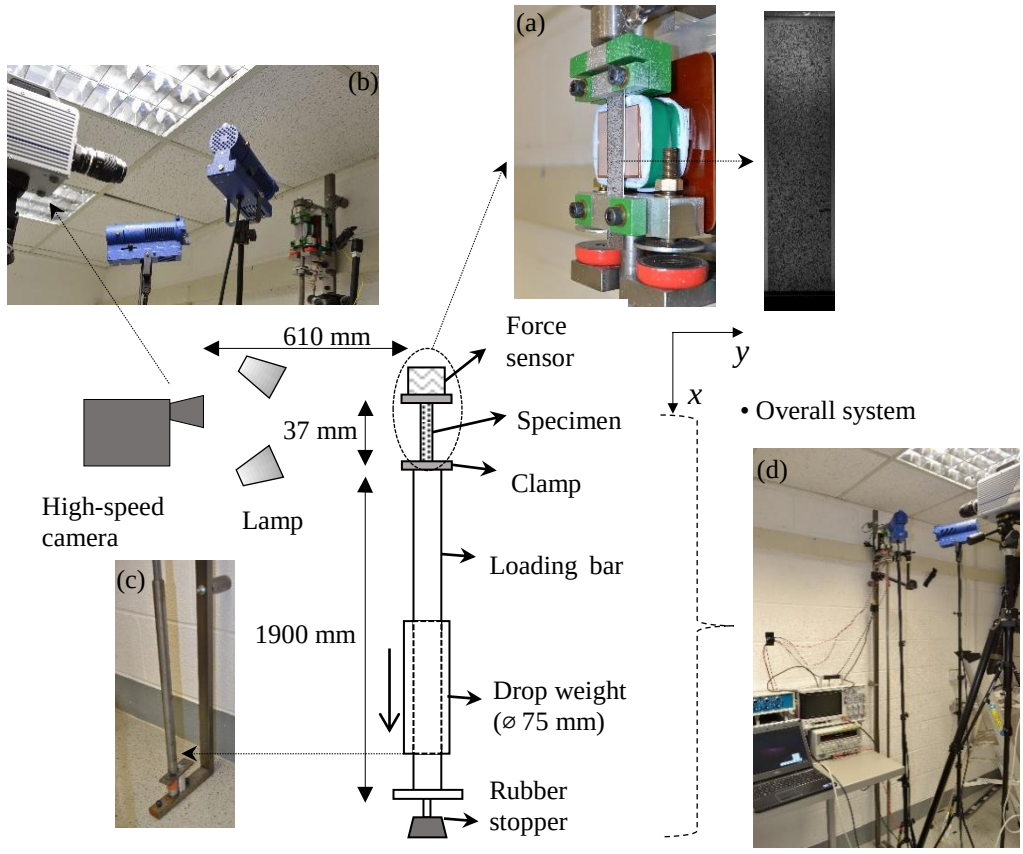

Figure 5. Schematic diagram of the drop-weight dynamic test and high-speed imaging system, showing actual pictures of (a) specimen between clamps, (b) imaging devices, (c) drop weight and (d) overall system (a stationary specimen picture taken by a high-speed camera is also given).

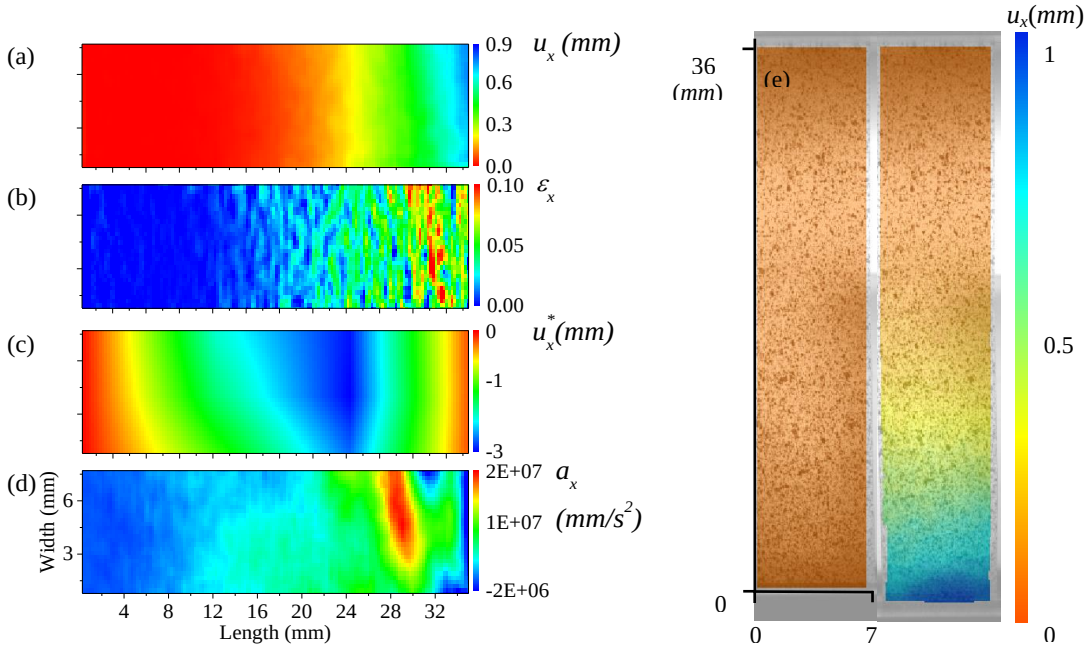

Figure 6. (a) Axial displacement, (b) true strain, (c) virtual displacement, (d) acceleration fields of the non-pre-stretching test at 0.3 ms and (e) the same axial displacement field overlaid on the actual picture (before and after loading) (SET1: non-pre-stretching).

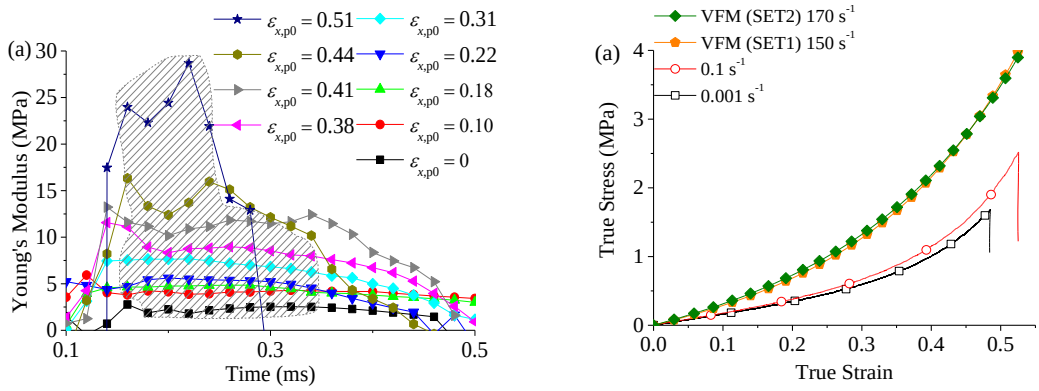

Figure 7. Left: Modulus identification at different strains from a silicone elastomer. Greyed area indicates the region over which the modulus was averaged for subsequent model fitting. This region is selected using a criterion on the identified Poisson's ratio. Right: Final stress-strain curves using identified material parameters, comparison to quasi-static data; strain rates are shown in the legend.

2.3 The non-linear VFM and large strain experiments

See also Yoon thesis chapter 6 and papers B, F, H

The procedure described so far has two particular weaknesses: there is a possibility that relaxation between the static and dynamic loads will alter the dynamic response (this is discussed in Yoon's thesis chapter 7 and paper G); and the experiment must be repeated a number of times. To address this, a large strain experiment was designed. Theoretically, this requires the integration of a non-linear constitutive model into the dynamic VFM, this has been done by previous authors for static loading, and their work was used as the basis of the method adopted in this project (Yoon thesis section 6.2, paper B). Experimentally, large strain loading was introduced by applying a larger velocity to the mobile end of the specimen, and allowing the stress wave to reverberate in the specimen: reverberation from high impedance boundaries preserves the sign of the stress, so that the tensile loading increased in a stepwise manner.

The procedure was first applied in a FE simulation, which again allowed the robustness of the analytical analysis and Matlab implementation to be confirmed, before moving on to experimental data. Noise studies were also performed, in addition to a study of the effect of rate dependence and sensitivity to specimen properties. The approach used in the non-linear implementation is to minimise an objective function with respect to the material parameters: the one term Ogden model was again used with an effective Poisson's ratio of 0.5 (an incompressible material). A typical output is given in Figure 8; a key point to note here is that until the first wave reflection in the specimen, at about 0.45 ms, the strain hardening parameter is identified as 0, and the modulus is too high: because only one stress state is experienced there is no mathematical difference between a stiffer material which doesn't harden, and a less stiff material which does. The second reflection gives additional information, in the form of a new stress state, which allows the strain hardening and stiffness to be correctly identified. It is noted that the Poisson ratio, which is purely geometric, is correctly identified early in the loading.

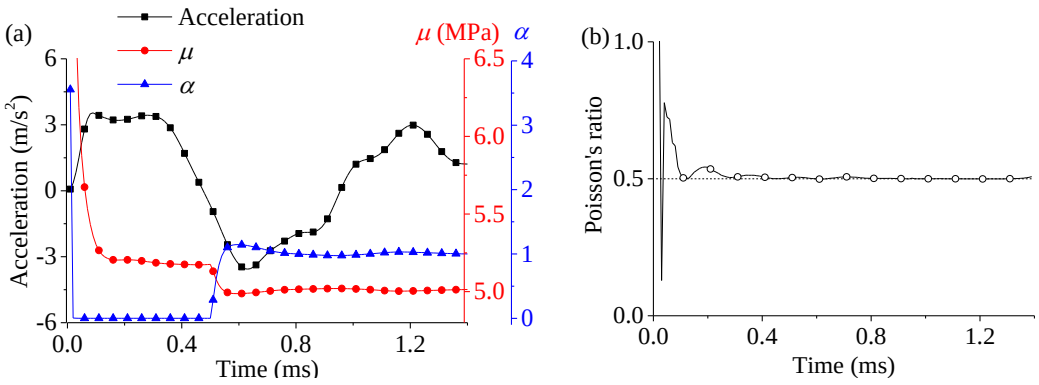

Figure 8. (a) Averaged acceleration profile and history of μ, α and (b) Poisson's ratio identifications obtained from the linear VFM. Given values were 5 MPa, 1 and 0.5 respectively.

Following a thorough investigation of the effects of noise and specimen geometry, experiments were performed. In order to provide the required long duration loading, the specimen was deformed using a gas gun system in which an aluminium block was given a large momentum and used to stretch the specimen, Figure 9. Further discussion of experimental parameters, including image correlation parameters is given in Yoon's thesis section 6.4.3. Example images, displacements, strains and accelerations are shown in Figure 10.

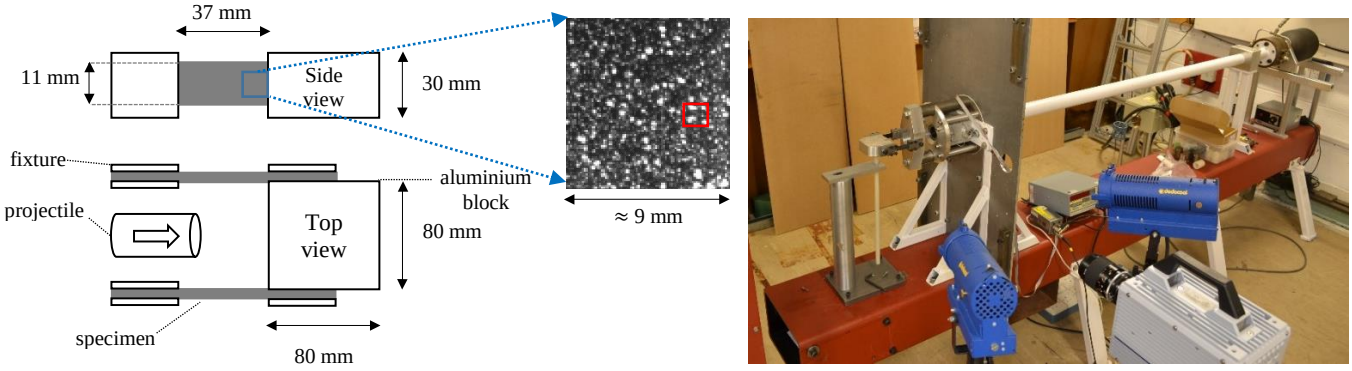

Figure 9. Left: Schematic representation of the gas-gun experiment and a typical speckle pattern the specimen surface, the 12×12 correlation window used in subsequent analysis is also indicated (red rectangle). Right: a photograph of the gas-gun system

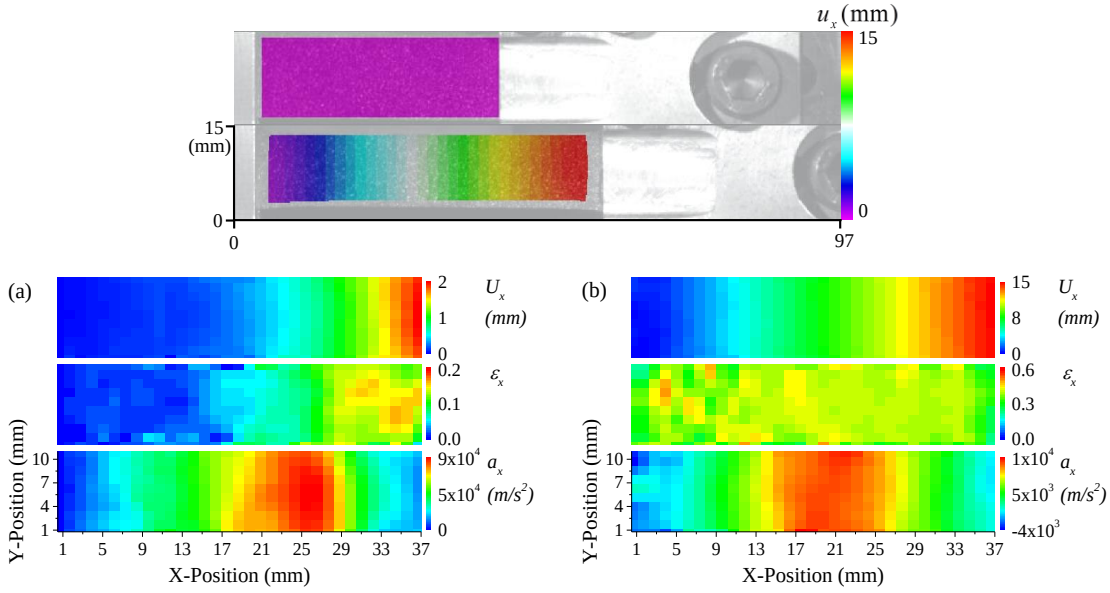

Figure 10. Top: Pictures of the initial and deformed states at 1.14 ms of TEST 3 and the axial displacement fields on the surfaces. Bottom: Axial displacement (upper), true strain (middle) and acceleration fields (bottom) at 0.34 and 1.14 ms of TEST 3.

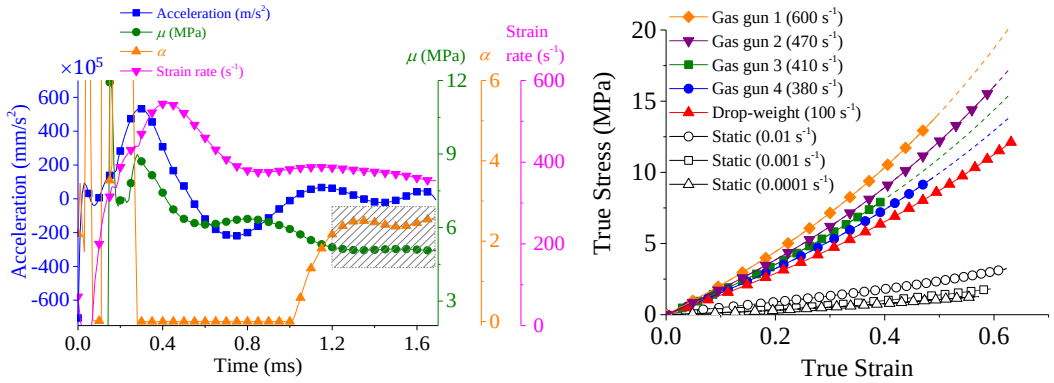

Figure 11. Left: Averaged acceleration and strain rate and history of μ and α prediction from gas-gun experiment on an EPDM specimen (TEST 3). Right: Ogden uniaxial true stress-strain curves reconstructed from the parameters of the gas-gun, drop-weight and quasi-static tests.

Estimates of μ and α were then produced using the procedure applied to the simulation output. Finally, these were used to reconstruct stress-strain curves, which are compared to data from the dropweight / linear VFM, and quasi-static experiments on the same material, Figure 11. Discussions of spatial and temporal smoothing are presented in Yoon's thesis section 6.5.

One weakness of this approach is that whilst the acceleration wavefront reflects from clamps there is a brief period during which the acceleration in the specimen is approximately zero. During this time, parameter identification may be interrupted. These periods become increasingly frequent with increasing strain, as the specimen becomes stiffer and the wave propagation speed increases. In order to address this, a new apparatus was built in which one of the clamps was monitored with a high frequency load cell. Information from this load cell was then combined with the acceleration information, recovering to some extent equation (1) and producing a more stable identification, Figure 12. This is discussed further in papers F and H, whilst paper H also discusses cyclic loading and the Mullins effect.

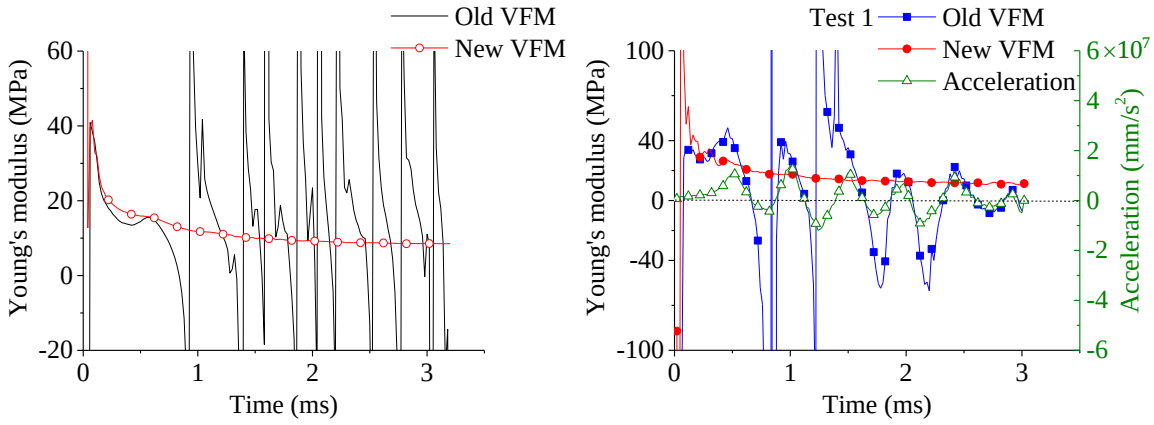

Figure 12. Comparison of VFM methods without and with force sensor information. The force sensor allows stable identification of modulus over a long period of time, even at those instances where the acceleration is zero. Note also that specimen relaxation can be identified.

2.4 Further Studies with the VFM

2.4.1 Comparison with compression data

Yoon thesis section 7.5.2, paper G

The Ogden strain energy potential can be used to derive stress-strain response in tension and compression using the same constitutive parameters. This gives the opportunity to compare the data obtained from the VFM with measurements made using a more conventional Hopkinson bar system. A titanium Hopkinson bar was used, in which stresses were measured directly at the bar specimen interfaces using piezoelectric stress gauges, and strains were measured using digital image correlation on the surface of the bars, along with the strain gauge signals. The advantage of applying the piezoelectric gauges and DIC is that very long duration experiments can be performed without the need to perform wave separation on the gauge signals. This system was used to produce compressive stress-strain curves for the material. These were compared to the compressive stress-strain response derived from the constitutive parameters obtained in the tensile tests, Figure 13. A similar comparison was performed for quasi-static data. In all cases, the compressive stresses were higher than those expected from the tensile response. FE simulations were then performed, which demonstrated that this discrepancy was consistent with a friction coefficient of 0.12 between the specimen and the loading anvils, which was accepted as a reasonable explanation.

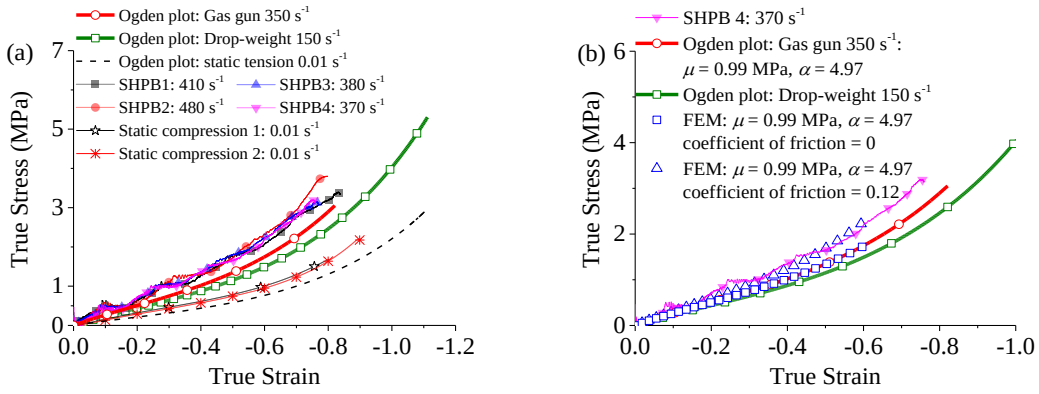

Figure 13. Left: Dynamic stress-strain curves in compression of pure silicone rubber: compression data from split Hopkinson bar tests (SHPB1-4) and two quasi-static tests; and the one-term Ogden plots calculated using data obtained from three sets of tensile experiments. Right: FEM simulations of compression experiments showing that the addition of friction moves the reconstructed Ogden plots to the same stress as the compression experiment.

2.4.2 Identification of Constitutive Models

Yoon thesis section 8.2

The experimental and analysis procedure in 2.2 produced a series of tangent moduli to a given material stress-strain relationship. In that section, these data were then used to produce the parameters of an optimised one-term Ogden model. More generally, however, rubbers may require models with more terms to be fully described, and the number of required terms may not be known. In order to address this, a procedure was developed to construct a global stress-strain curve from a series of segments generated at different pre-strains. These segments were produced using the dropweight apparatus with static pre-strains, but with the non-linear VFM implementation based on a one-term Ogden model. The segments were then 'connected' by shifting along the stress axis using an optimisation algorithm that assumed that the *local* non-linearity could be approximated by a one-term Ogden model, even if the *global* stress strain curve was better described by another hyperelastic formulation (e.g. 2-term Ogden, Mooney Rivelin), Figure 14. Finally, a suitable hyperelastic model could then be chosen based on consideration of the stress-strain relationship produced. The process was first developed using data from FE simulations, and then applied to experiments performed on nitrile rubber. However, when the experiments were performed at room temperature, there was a considerable difference between the stress-strain relationship produced using the new method and that produced using the method described in section 2.2, Figure 15. This difference was ascribed to a material relaxation, which caused a significant relaxation of the modulus on the timescale of the experiment (observable in Figure 15. top left). Further experiments at 62 °C, where the relaxation is no longer significant, along with FE simulation using a time-dependent material model confirmed this hypothesis, and led to the application of a time-dependent VFM, described in the next section.

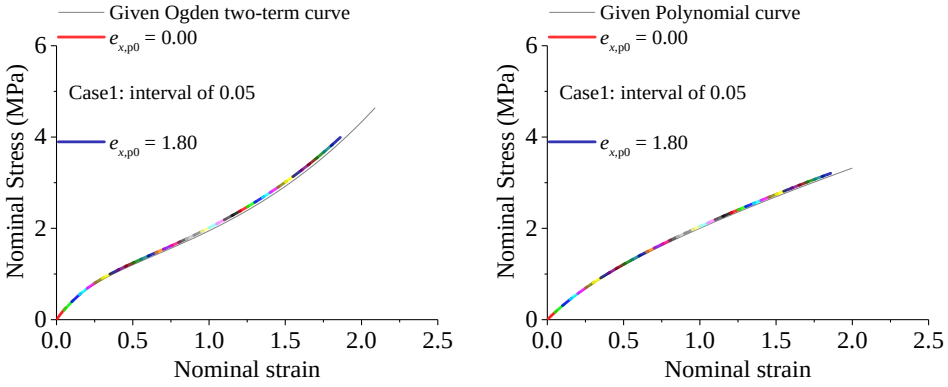

Figure 14. Reconstruction of stress-strain curves out of segments produced from dynamic loading superposed on different static pre-strains; pre-strains at intervals of 0.05. Left, input model was two-term Ogden. Right, input model was Mooney-Rivelin. All from FE simulation data

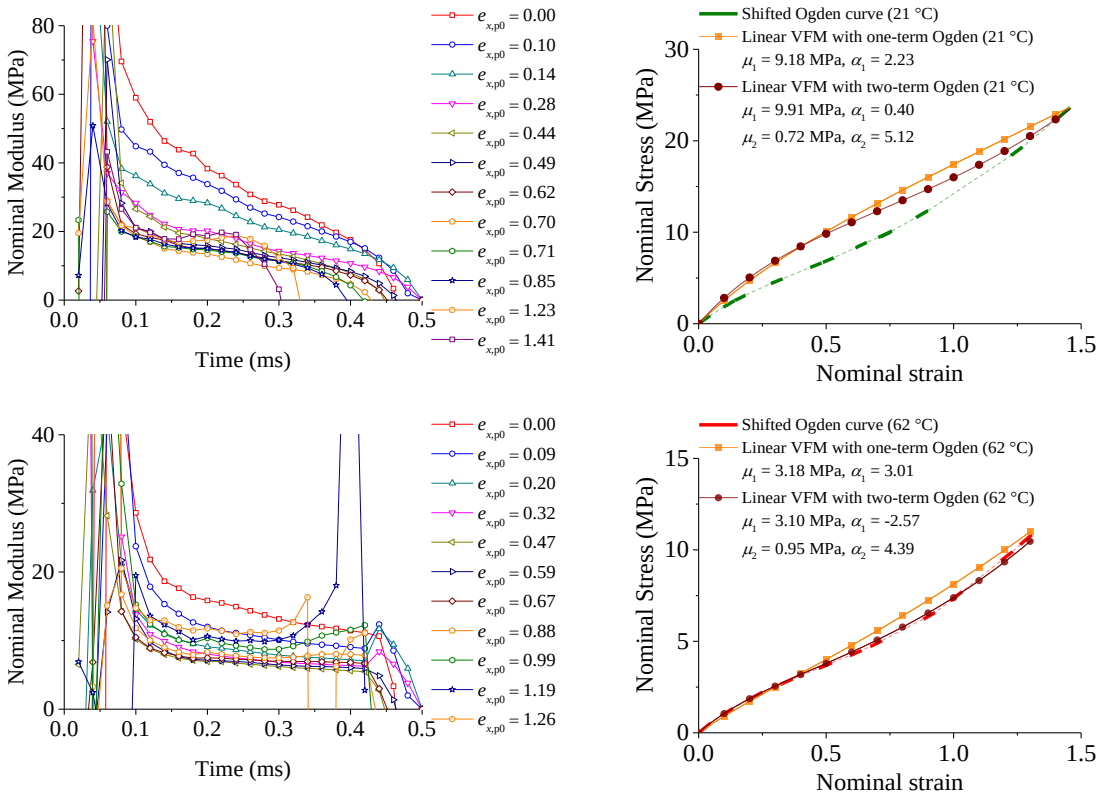

Figure 15. Top left: modulus identifications at different pre-strains, 21 °C; Top right: comparison of the curve produced using the new model independent shifting method (green), and those produced by optimising one and two term Ogden models to the experimental data. Bottom left: modulus identifications at different pre-strains, 62 °C; Bottom right: comparisons of new method and optimised curves.

2.4.3 Relaxation and temperature dependence

Yoon thesis chapter 8.3, paper A

The dropweight apparatus in section 2.2 was modified to give temperature control between c.a. -10 °C and +60 °C, and a time-dependent constitutive model implemented into the principle of virtual work equations described above using a 5-term Prony series with relaxation times from 10^{-5} to 10^{-3} s. The shorter of these times was chosen based on the framing rate of the camera (50 000 fps) and the longer on the duration of the experimental loading (1 ms).

To test the implementation, FE simulations were performed with both visco-hyperelastic (one-term Ogden) or linear viscoelastic models using 20 (Nitrile rubber) or 7 (Silicone rubber) term Prony series calibrated from DMA data. Hence, the input constitutive model had a more complete relaxation spectrum than the VFM analysis; as does the real material behaviour.

Simulations were performed at a number of temperatures. The output from a given simulation and analysis is a series of 5 parameters, which can then be used to construct a modulus-time curve between 10^{-5} and 10^{-3} s. Time temperature superposition was then used to produce a master curve which could be compared to the input data, Figure 16.

Experiments were performed on nitrile rubber and silicone rubber and analysed using an identical procedure to produce the results in Figure 17.

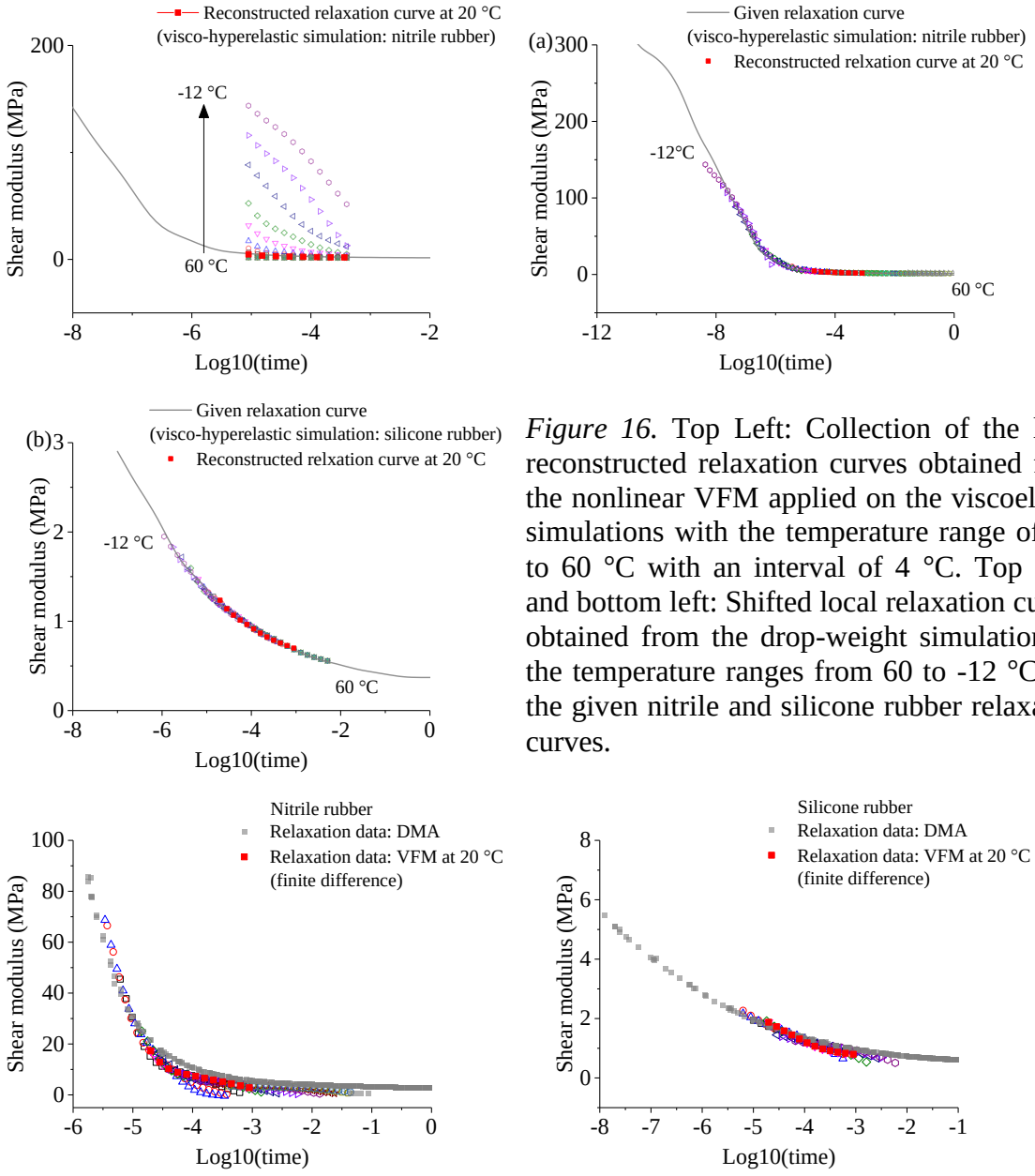

Figure 16. Top Left: Collection of the local reconstructed relaxation curves obtained from the nonlinear VFM applied on the viscoelastic simulations with the temperature range of -12 to 60 °C with an interval of 4 °C. Top right and bottom left: Shifted local relaxation curves obtained from the drop-weight simulations at the temperature ranges from 60 to -12 °C and the given nitrile and silicone rubber relaxation curves.

Figure 17. Shifted local relaxation curves obtained from drop-weight experiments compared to relaxation curves obtained from the DMA (finite difference refers to the method used to calculate specimen acceleration fields).

3 Rod and Interface Techniques: Methods, Assumptions, Procedures and Results

3.1 Background, waves in slender rods

Dynamic loading of a long slender rod produces a stress wave that propagates approximately according to the 1D wave equation

$$\frac{\partial^2 u}{\partial t^2} = \frac{E}{\rho}\frac{\partial^2 u}{\partial x^2}, \tag{6}$$

where u is the particle displacement, x the position along the rod and t is time, whilst E is the Young's modulus and ρ the density of the rod material (see [9]). Solutions to this equation are waves propagating at a speed of $c = \sqrt{E/\rho}$ in both the positive and negative x directions, i.e.

$$u(x,t) = u_0 e^{\pm \alpha x} e^{i(\omega t \pm \kappa x)}, \tag{7}$$

where ω is the frequency of a wave component, and κ the wavenumber. Here we consider only the wave travelling in the positive x direction, for which the signs in the exponents are both '-'. Hence, the term u_0 represents the amplitude of the wave at some arbitrary location and time which we define as $x = 0$ and $t = 0$, the term $e^{i(\omega t - \kappa x)}$ gives a wave propagating at speed $c = \omega/\kappa = \sqrt{E/\rho}$, and the term $e^{-\alpha x}$ represents the decrease in amplitude if there is damping owing to energy dissipation in the material. This expression represents a sinusoidal wave of frequency ω; in linear materials all other wave shapes can be expressed as a Fourier series.

Experimentally, the propagation of this wave is most readily measured using surface mounted strain gauges. The expression for the wave in terms of strain is

$$\varepsilon(x,t) = \varepsilon_0 e^{\pm \alpha x} e^{i(\omega t \pm \kappa x)}, \tag{8}$$

where ε_0 represents the strain at $(x,t) = (0,0)$. Hence, if we make multiple measurements of strain at different points in the rod, say x_1 and x_2, we can calculate the wave propagation parameters as

$$\alpha = \frac{\ln\left|\dfrac{\varepsilon(x_1,t)}{\varepsilon\left(x_2, t + c(x_2 - x_1)\right)}\right|}{x_2 - x_1}. \tag{9}$$

$$\kappa = \frac{angle\left[\dfrac{\varepsilon(x_1,t)}{\varepsilon\left(x_2,t+c(x_2-x_1)\right)}\right]}{x_2-x_1}. \tag{10}$$

The equations so far have been derived for a single frequency; since any realistic impact loading induces waves of multiple frequencies, there is an opportunity to obtain frequency dependent information by taking Fourier transforms of the strain signals, $\tilde{\varepsilon}(x,\omega)$, and using

$$\alpha(\omega) = \frac{\ln\left|\dfrac{\tilde{\varepsilon}(x_1,\omega)}{\tilde{\varepsilon}\left(x_2,\omega\right)}\right|}{x_2-x_1}. \tag{11}$$

$$\kappa(\omega) = \frac{angle\left[\dfrac{\tilde{\varepsilon}(x_1,\omega)}{\tilde{\varepsilon}\left(x_2,\omega\right)}\right]}{x_2-x_1}. \tag{12}$$

to give frequency dependent values of the damping coefficient, α, and the wavenumber κ.

It now remains to relate α and κ to material properties. This can be done in both a material dependent and material independent framework. Examples for common models of linear viscoelasticity (Maxwell, Voigt, SLS) are given in Huang's Thesis, the general results for the complex modulus $E^* = E' + iE''$ are

$$E'(\omega) = \frac{\rho\omega^2(\kappa^2-\alpha^2)}{(\kappa^2+\alpha^2)^2}, \tag{13}$$

$$E''(\omega) = \frac{\rho\omega^2\times 2\kappa\alpha}{(\kappa^2+\alpha^2)^2}. \tag{14}$$

Note that for undamped materials, as $\alpha\rightarrow 0$, $E'(\omega) = \rho\omega^2/\kappa^2 = \rho c^2$, as required.

Before moving to a discussion of the experimental strain measurements and subsequent analysis, it is important to note that in practice slender rods exhibit geometric dispersion. Owing to the Poisson effect, no wave propagates under a state of uniaxial stress: as the wave passes, the material is deformed radially as well as longitudinally. This adds a radial component to the dynamic equilibrium equation that is solved to produce equation (6), and alters the wavespeed. In practice, the effect is small for wavelengths longer than c.a. 10 bar diameters. Dispersion effects are considered in this project, but are shown in most cases to be small.

3.2 Overview of experimental procedure for single rod method

An apparatus was constructed in which a slender rod (length c.a. 1 m, diameter c.a. 13 mm) was held in low friction bearings and impacted at low speeds using a pendulum. A number of different impactors could be inserted into the pendulum, in most cases spheres were used as these were found to give the broadest range of frequencies. The rod was instrumented halfway along its length with four surface strain gauges mounted at 90 degree intervals; these were then combined in a bridge arrangement to cancel strains resulting from bending, and amplified using a commercial strain gauge amplifier with a stated bandwidth of 500 kHz. Later analysis showed that the highest frequencies present in our experiments were of the order 20-30 kHz. Both ends of the rod were unconstrained, so that the wave would reflect multiple times, alternating between compression and tension as it did so. The single gauge station was used to measure the strain-time profile in the rod during this time, by ensuring that the spatial extent of the wave was less than 1 m, these measurements could be interpreted as the multi-point values required in the above analysis, with the advantage that as the same gauges were used for all measurements, no gauge calibration was required.

Although not discussed here, an extensive programme of Finite Element simulations was performed. The simulations replicated exactly the experimental conditions, material models used were an elastic material with the same properties as the Titanium alloy Ti6Al4V, and a linear viscoelastic model with a Prony series calibrated to DMTA measurements on PMMA. Strains were extracted from the model at the gauge location, and then analysed using the same Matlab code as the subsequent experiments. Hence, the FE simulations gave a confirmation of both the analytically derived equations and the Matlab implementation, whilst also providing a test-bed in which effects such as pulse duration and frequency content, bar dimensions, and dispersion correction could be investigated. These investigations are described in detail in Huang's thesis.

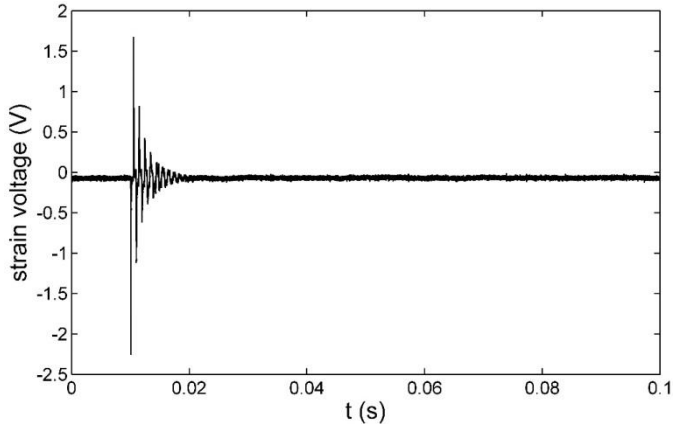

Figure 18. Strain gauge recording from a 1m long, 13 mm diameter PMMA rod impacted using a 12.5 mm diameter PMMA ball at a temperature of 17.5 °C.

A typical strain gauge recording from a test on a PMMA rod is given in Figure 18. The first step of the analysis is to identify the individual strain pulses in the signal. A number of identification methods were used, and are discussed in Huang's thesis; the signals are shown in more detail in Figure 19. These signals are now extracted, and are time shifted so that their peak is at the centre of a record of 0.1s duration: to achieve this, the pulses padded on each side with zeros, Figure 20. The cantering and zero padding help to interpret the Fourier transforms later in the data analysis process (see Huang's thesis). Dispersion correction is then applied, and the FFT function in Matlab is used to calculate the discrete Fourier transforms of the pulses, Figure 21. Finally, the equations above are used to calculate the two wave propagation coefficients, α and κ, and hence the wavespeed c (remembering to account for the time shifting when calculating κ), from which E', E'' and their ratio, tanδ may be found, Figure 22.

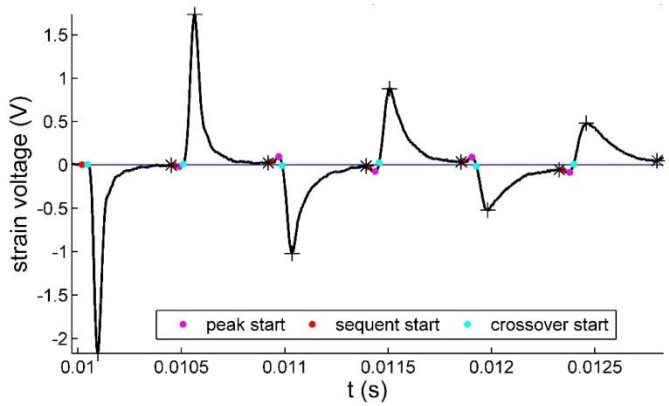

Figure 19. Strain signals from the experiment in Figure 18, indicating start and end locations of individual pulses chosen by different methods.

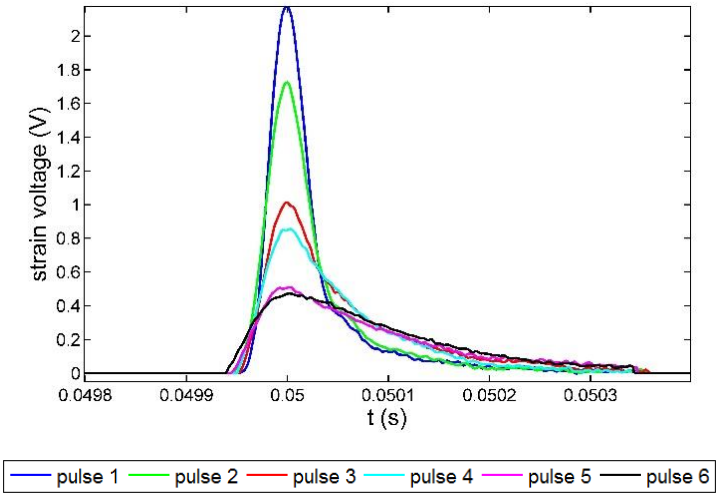

Figure 20. Extracted and time-shifted signals from Figure 19.

Figure 22 shows the basic output of the analysis. Here, experiments have been performed using the same rod and impactor, at a number of different drop heights, representing a change in impact speed of a factor of approximately 1.5. The data indicate that the material is in the linear viscoelastic regime at all times: the results do not depend on drop height. The data are very consistent below a frequency of 20 kHz, but highly inconsistent above this. This is attributed to there being very little energy, and hence information, contained in the wave at frequencies above 20 kHz. The Fourier transforms are of single pulses, and contain information down to 0 Hz; however, the lowest natural frequency of the rod is approximately 2000 m s^{-1} / 1m = 2 kHz, and this is used as an estimate of the lowest useful frequency.

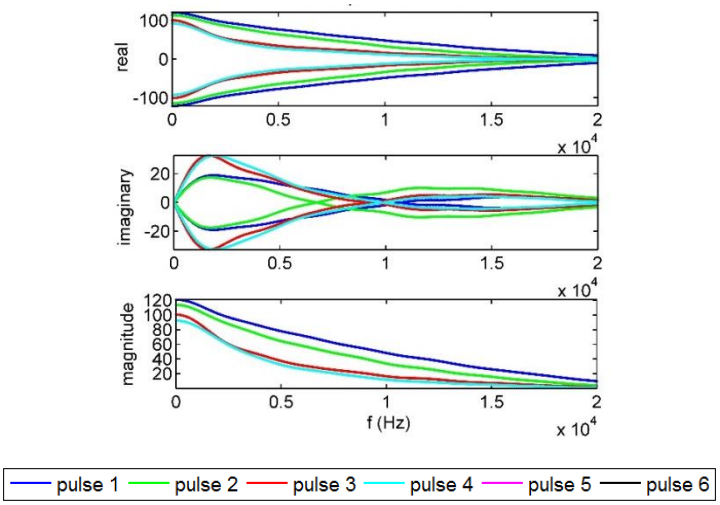

Figure 21. Fourier Transforms of the pulses in Figure 20

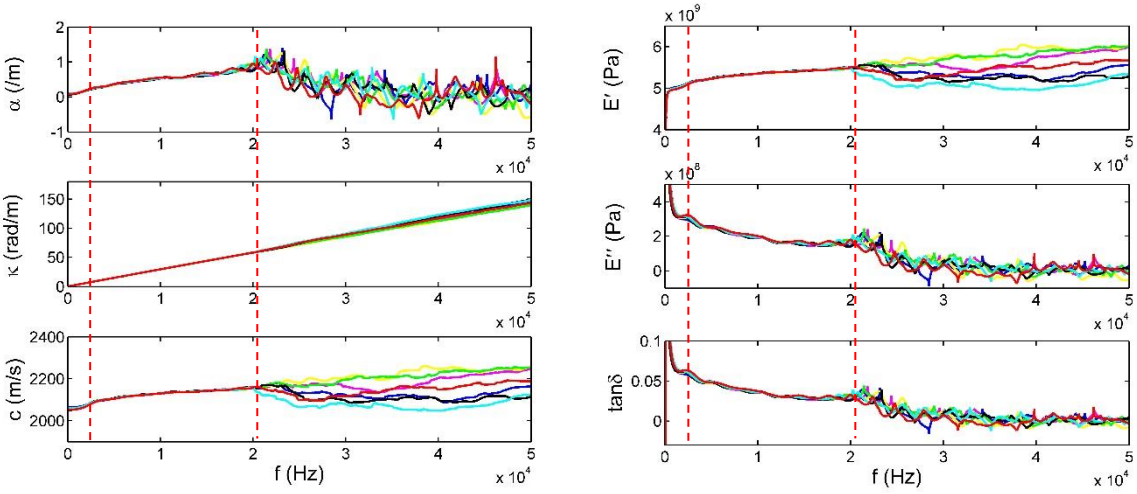

Figure 22. Propagation coefficients and moduli calculated from a number of experiments on a1m long, 13 mm diameter PMMA rod impacted using a 12.5 mm diameter PMMA ball at a temperature of 17.5 °C.

3.3 Summary of Results from Single Rod Method

3.3.1 Titanium alloy

Experiments were performed on a 12.7 mm diameter Titanium alloy (Ti6Al4V) rod of length 1 m. The derived material response is shown in Figure 23, and as expected the storage modulus is approximately 110 GPa and the loss modulus is close to zero. These experiments were performed using the same 12.5 mm diameter PMMA impactor as the PMMA experiments shown above, indicating that the bandwidth of the pulse depends on the rod material as well as the impactor (and details of the impactor-rod interaction which were not explored fully).

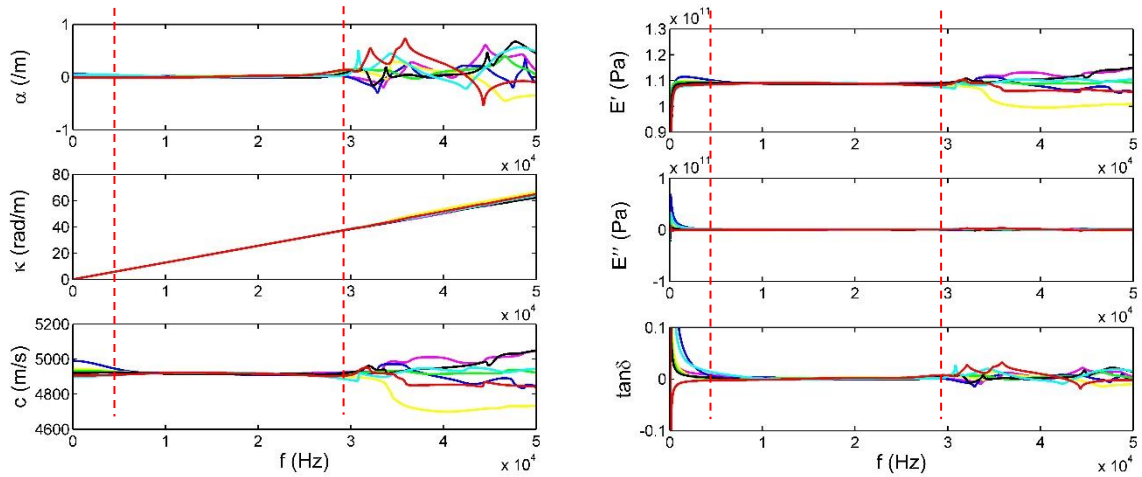

Figure 23. Derived propagation coefficients and moduli from Titanium rod impact tests

3.3.2 PMMA

Experiments were performed using different impactor materials and speeds, and different temperatures. The derived material properties were independent of impactor type and speed, but were sensitive to temperature even over a small range, Figure 24, emphasising the importance of keeping accurate temperature records when performing experiments on polymers. Further measurements of wave propagation were performed using a laser vibrometer to monitor the longitudinal velocity of one of the free ends of the rod. These were again used to derive material properties. The agreement with the strain gauge signals was good, but there is a statistically significant difference in the attenuation coefficients calculated, which affects the loss modulus in particular and may warrant further investigation, Figure 25. Finally, data were compared to values obtained from DMTA measurements of storage and loss modulus, shifted to appropriate frequencies using time-temperature superposition, Figure 26. Again, the agreement is good, but may warrant further investigation. In this case, it is not clear whether the differences are as a result of the rod measurements, the DMA measurements, or both. Significant further discussion of this technique may be found in Huang's Thesis.

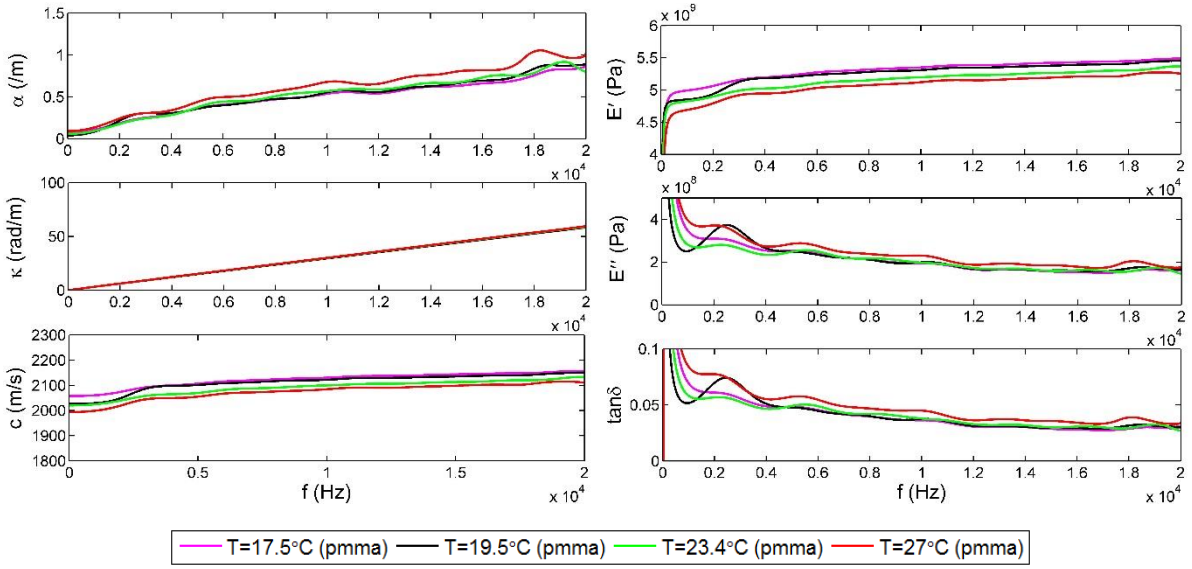

Figure 24. Propagation coefficients and moduli for PMMA at different temperatures

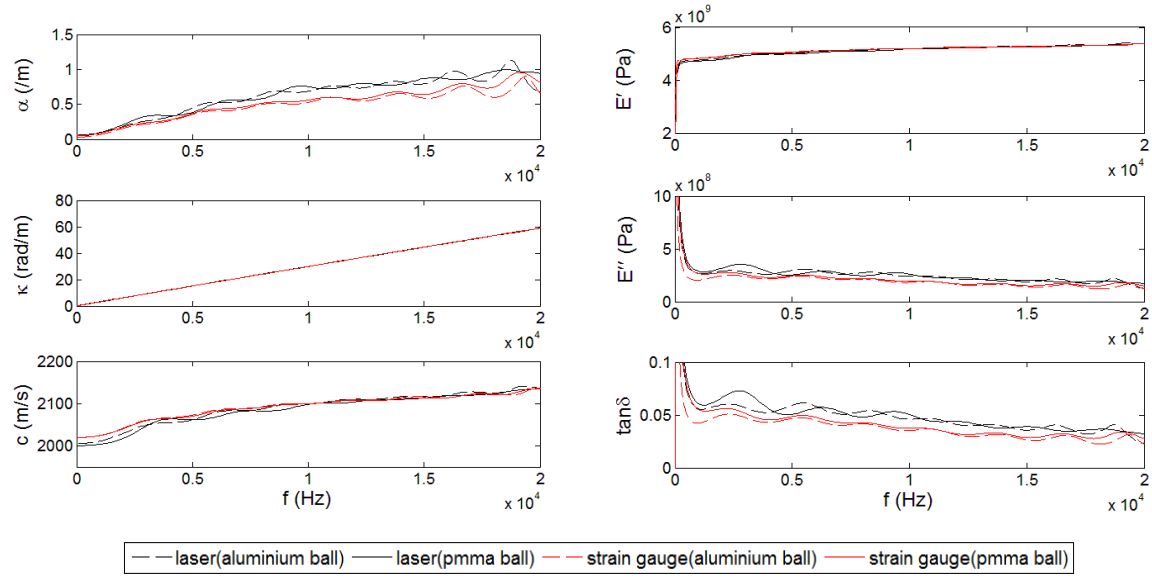

Figure 25. Comparison of strain gauge-based and laser vibrometer-based results from a PMMA rod impacted with 12.3 mm aluminium ad 12.5 mm PMMA ball impactors.

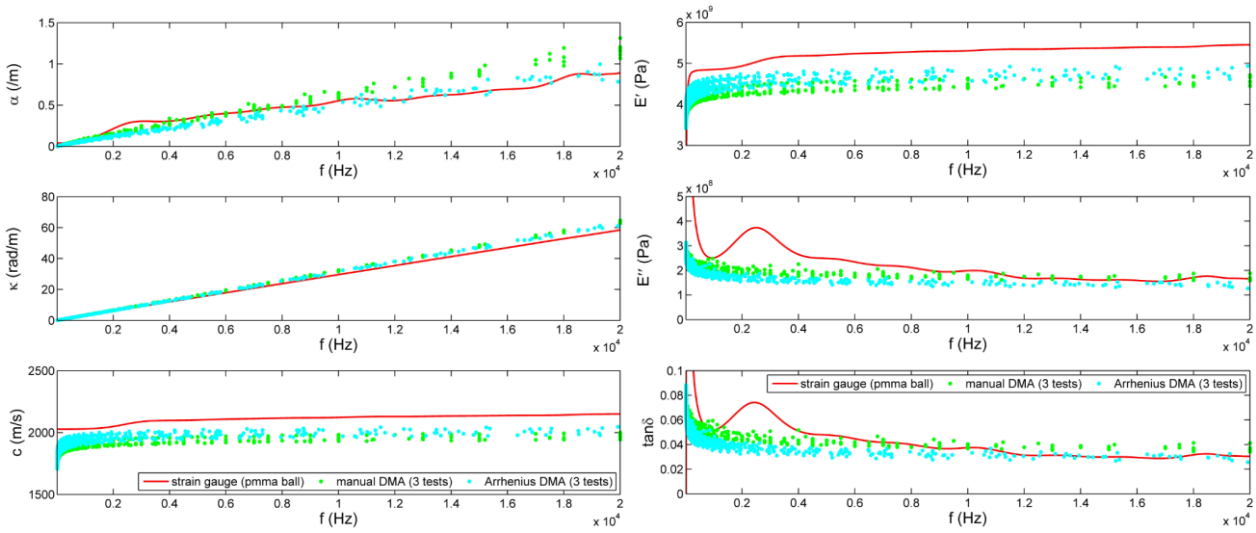

Figure 26. Comparison of results derived from single rod impact tests and time-temperature shifted DMA tests (19.5 °C). Wave propagation coefficients (left hand side) are obtained directly from the rod impact experiments, but derived from the DMA data. Moduli (right hand dise) are obtained directly from the DMA, but derived from the rod impact experiments.

3.4 Background: waves at rod interfaces

When a stress wave reaches an interface between two materials with different impedances, some of the wave is reflected and some transmitted; the fractions of energy that do each are governed by the relative impedances of the materials. In the case of boundaries between slender rods laid end to end, the relevant impedance is the mechanical impedance, Z, given for each rod by

$$Z = \sqrt{E * \rho}\, A\,, \tag{15}$$

where A is the area of the rod. Hence, in principle it is possible to identify the frequency dependent mechanical properties of an unknown material by monitoring the behaviour of a stress wave at a boundary between a slender rod of that material, and another rod whose properties are known. Here the relevant mathematics for solving this problem will be summarised in a model independent framework; further information is available in Huang's Thesis.

We start by assuming that the particle velocity and force are continuous across the interface. This is true of glued interfaces; we will also assume that it is true of interfaces under compressive loads, although it is possible to imagine interface separation under certain conditions when subsequent unloading takes place. If we define the system so that an incident wave propagates along an input rod and then interacts with a boundary between that and an output rod, there are two waves in the input rod: the wave travelling towards the interface, I and the

reflected wave *R*; and one wave in the output rod, *T*. The particle velocities and forces induced in the rods may be written as a linear combination of the waves, such that the boundary conditions become

$$\begin{aligned} \dot{u}_I(0,t) + \dot{u}_R(0,t) &= \dot{u}_T(0,t) \\ F_I(0,t) + F_R(0,t) &= F_T(0,t) \end{aligned}, \tag{16}$$

where we have arbitrarily stated that the interface is at $x = 0$. In practice, the waves are measured using strain gauges remote from the interface, so that

$$\begin{aligned} u_I &= u_{I0} e^{i\omega t} e^{-\gamma_1 x_I} \\ u_R &= u_{R0} e^{i\omega t} e^{\gamma_1 x_R} \\ u_T &= u_{I0} e^{i\omega t} e^{-\gamma_2 x_T} \end{aligned}, \tag{17}$$

where $\gamma_{1,2} = \alpha_{1,2} + i\kappa_{1,2}$ is called the propagation coefficient, and represents the properties we seek in the input (1) and output (2) bars. Here, x_I, x_R and x_T are the locations of the gauges, and in practice $x_I = x_R$.

As with the wave propagation measurements, these equations are valid for any frequency, and if the material used is linear, an arbitrary wave can be constructed as a Fourier series, again allowing frequency dependent properties to be derived from Fourier transforms. However, conversion to different quantities (e.g. strain, force, stress etc) is more complicated, as we are no longer taking ratios of waves in the same material. In practice, we wish to use the strain, which is the spatial derivative of the displacement equations above. We can take the spatial and temporal derivatives of equations (17), and define the Transmission and Reflection coefficients, TC and RC as the ratios of the strains induced by the Transmitted and Reflected waves to that induced by the Incident wave. Finally, using the two boundary conditions defined in equations (16) give two expressions to calculate the ratio of material properties of the input and output bars, which may be applied to the Fourier transforms of the strain-time data from the gauges:

$$\frac{\gamma_2}{\gamma_1} = \frac{TC_{\hat{\varepsilon}}(x_I, x_T, \omega) \times e^{\gamma_2 x_T - \gamma_1 x_I}}{1 - RC_{\hat{\varepsilon}}(x_I, x_R, \omega) \times e^{-(\gamma_1 x_R + \gamma_1 x_I)}}, \tag{18}$$

$$\frac{\gamma_2^2}{\gamma_1^2} = \frac{S_2}{S_1}\frac{\rho_2}{\rho_1}\frac{TC_{\hat{\varepsilon}}(x_I, x_T, \omega) \times e^{\gamma_2 x_T - \gamma_1 x_I}}{1 + RC_{\hat{\varepsilon}}(x_I, x_R, \omega) \times e^{-(\gamma_1 x_R + \gamma_1 x_I)}}, \tag{19}$$

Where we note that: either equation can be used to solve for the propagation coefficient of either bar in terms of that in the other; in principle, it is possible to combine both equations to eliminate either TC or RC (this is straightforward for elastic bars): and the equations must be solved numerically.

3.5 Implementation and FE validation: waves at rod interfaces

Significant discussion of the above equations is presented in Huang's thesis. In order to test the Matlab implementation, Finite Element simulations were constructed using both elastic and viscoelastic materials, examining, in particular, effects of gauge location. As an example, simulation results are here shown for a simulated interface between Ti6Al4V and PMMA. Numerical solvers were used, but because the propagation coefficients (γ) are complex, there is an infinite number of solutions for κ and suitable constraints must be used; the tightness of these constraints increases as the gauge on the output bar moves further from the interface. Errors were also introduced by the contact algorithms in Abaqus, especially when using equation (18), which is derived from displacement continuity at the interface. Further simulations were performed using a single rod made from two materials, eliminating the need for contact algorithms and demonstrating that the error was associated with the FE simulation, not the analysis. The analysis procedure is demonstrated in Figures Figure 27 to Figure 30.

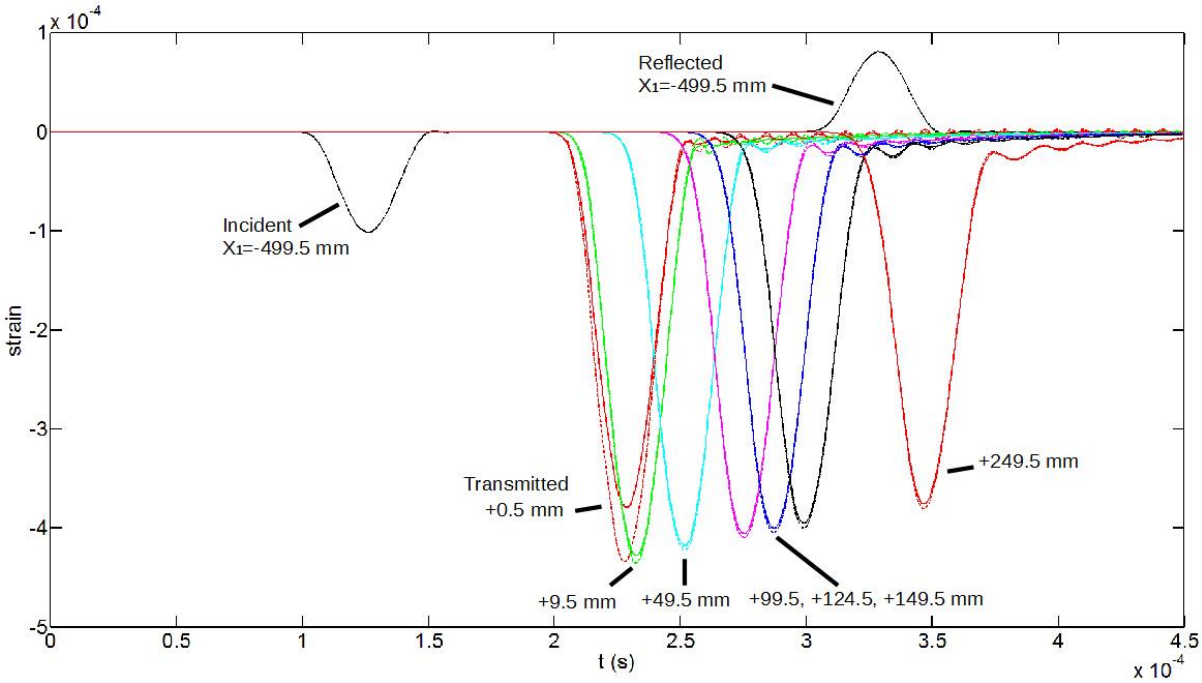

Figure 27. Incident, reflected and transmitted waves from FE simulation of wave propagation between Ti64 and PMMA rods. The incident and reflected waves are measured 499.5 mm from the interface; the transmitted wave at a number of locations. Note that we would prefer to measure as close to the interface as possible, but at too small a distance the strain on the rod surface (solid line) is not the same as that in the centre of the rod (dashed line).

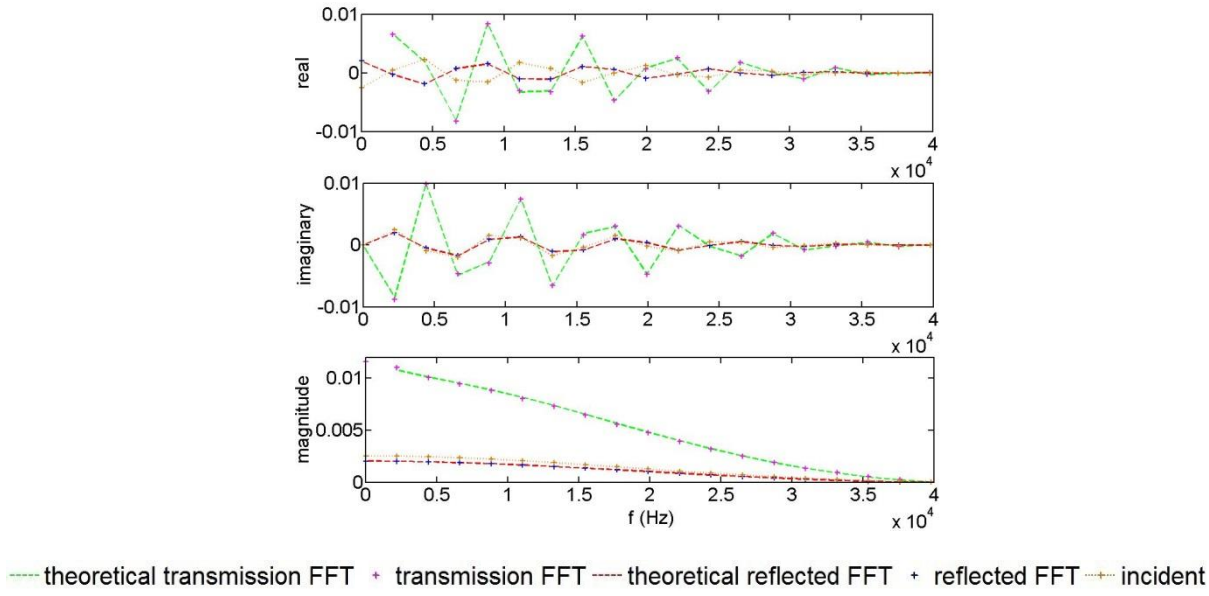

Figure 28. Comparisons of FFTs of the FE reflected and transmitted waves from Figure 27 and those expected from an analytical analysis (labelled 'theoretical'). Transmitted wave at 124.5 mm.

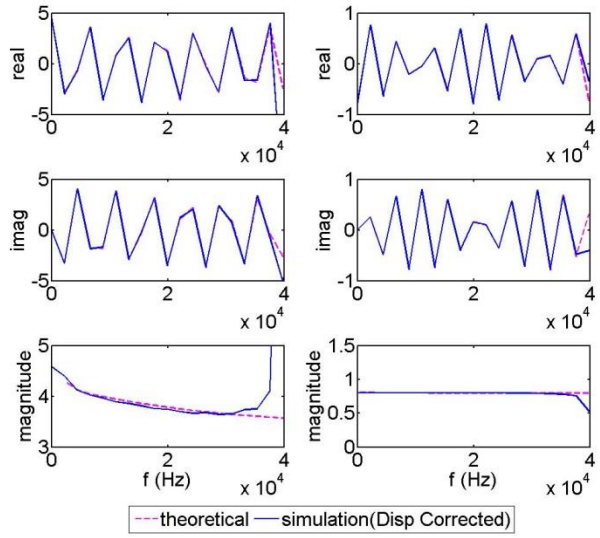

Figure 29. Transmission (left) and Reflection Coefficients (right) calculated from data in Figure 28.

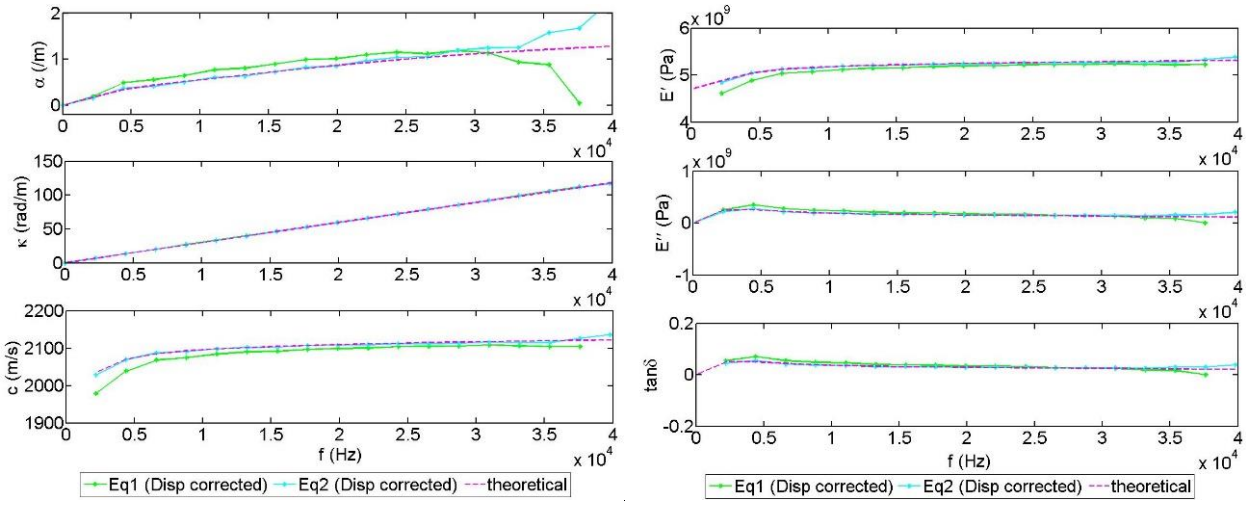

*Figure 30.*Material properties derived from data in Figure 29. Equation 1 refers to the velocity boundary condition (13) and equation 2 to the force boundary condition (14). The error in Equation 2 is associated with the contact conditions in the FE simulation, and was removed when a simulation was performed using a single rod with two materials.

3.6 Experimental data: waves at rod interfaces

In keeping with the FE simulations, experiments were first performed using single rods with two gauge stations. Because the rods were of a single material, a 'virtual' boundary could be ascribed anywhere in the rod, and the transmission coefficient was necessarily equal to 1. Experiments were performed to test effects of various potential sources of error, including measurements of distance between the gauges, and differences in effective gauge factor. Results from these experiments are outlined in Figure 31 and Figure 32. Finally experiments were performed on real interfaces between Ti and PMMA rods. Transmission and Reflection coefficient data from these experiments are shown in Figure 33. These data show that although the current implementation of the technique is able to produce reasonable estimates of the modulus to high frequencies (about 50 kHz), work is required to improve the precision of these measurements. The larger errors are in the calculations of the transmission coefficient, and work is ongoing to identify whether calculating the transmitted material parameters from the reflection coefficient alone gives improved results: or whether the calculation would be more sensitive to the smaller errors. Given that accurate results were derived from the 'virtual' boundary, it is expected that the errors are, in fact, associated with boundary effects at the ends of the two bars. These possibilities are being explored in more detail in the preparation of Huang's thesis.

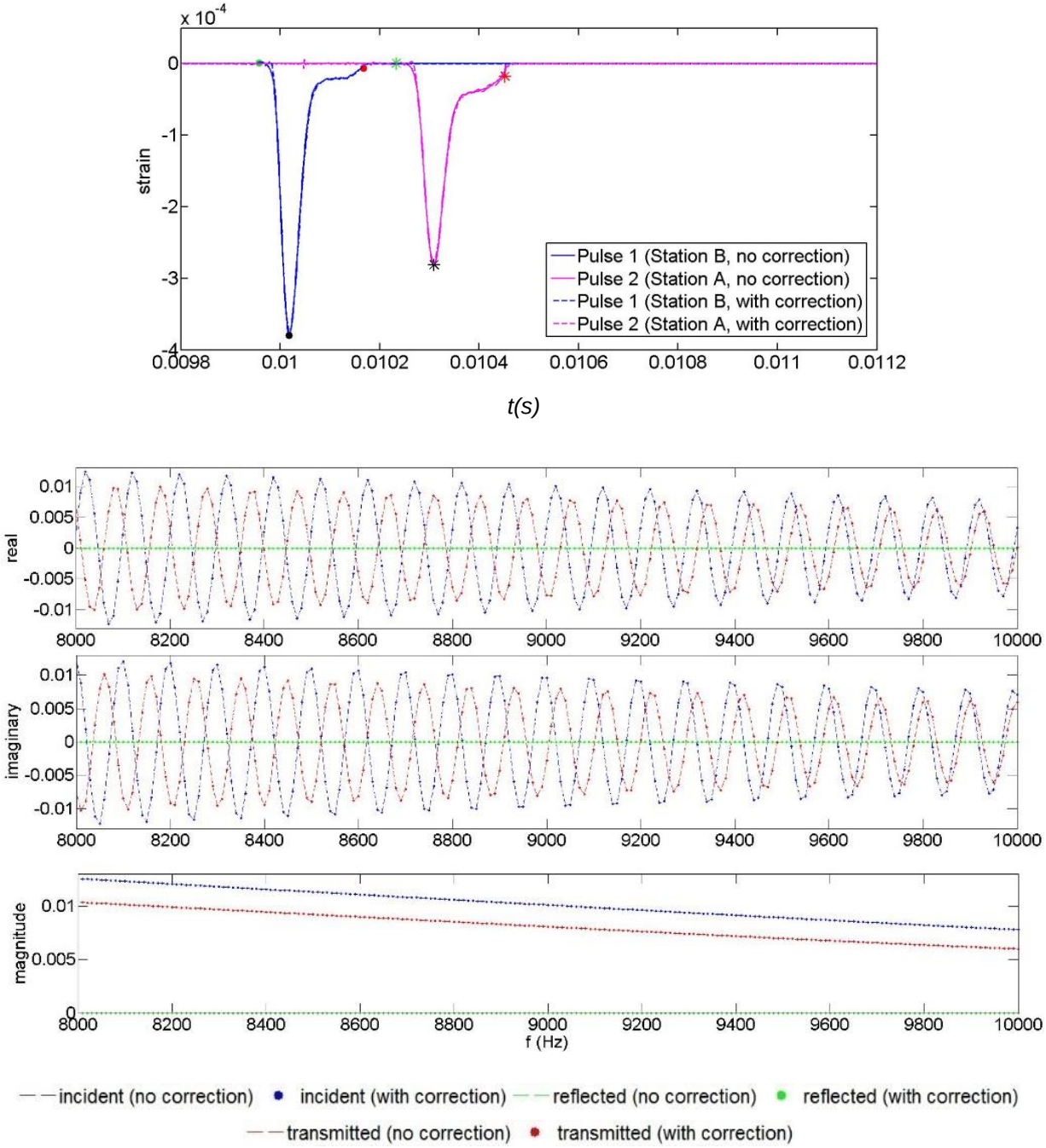

Figure 31. Top: Raw strain signals obtained from two gauge stations on a single rod of PMMA. Bottom, Fourier transforms of the signals; both cases the small effect of dispersion correction is shown. The reflected signal is zero because there is no interface. Figure only shows a small frequency range for clarity.

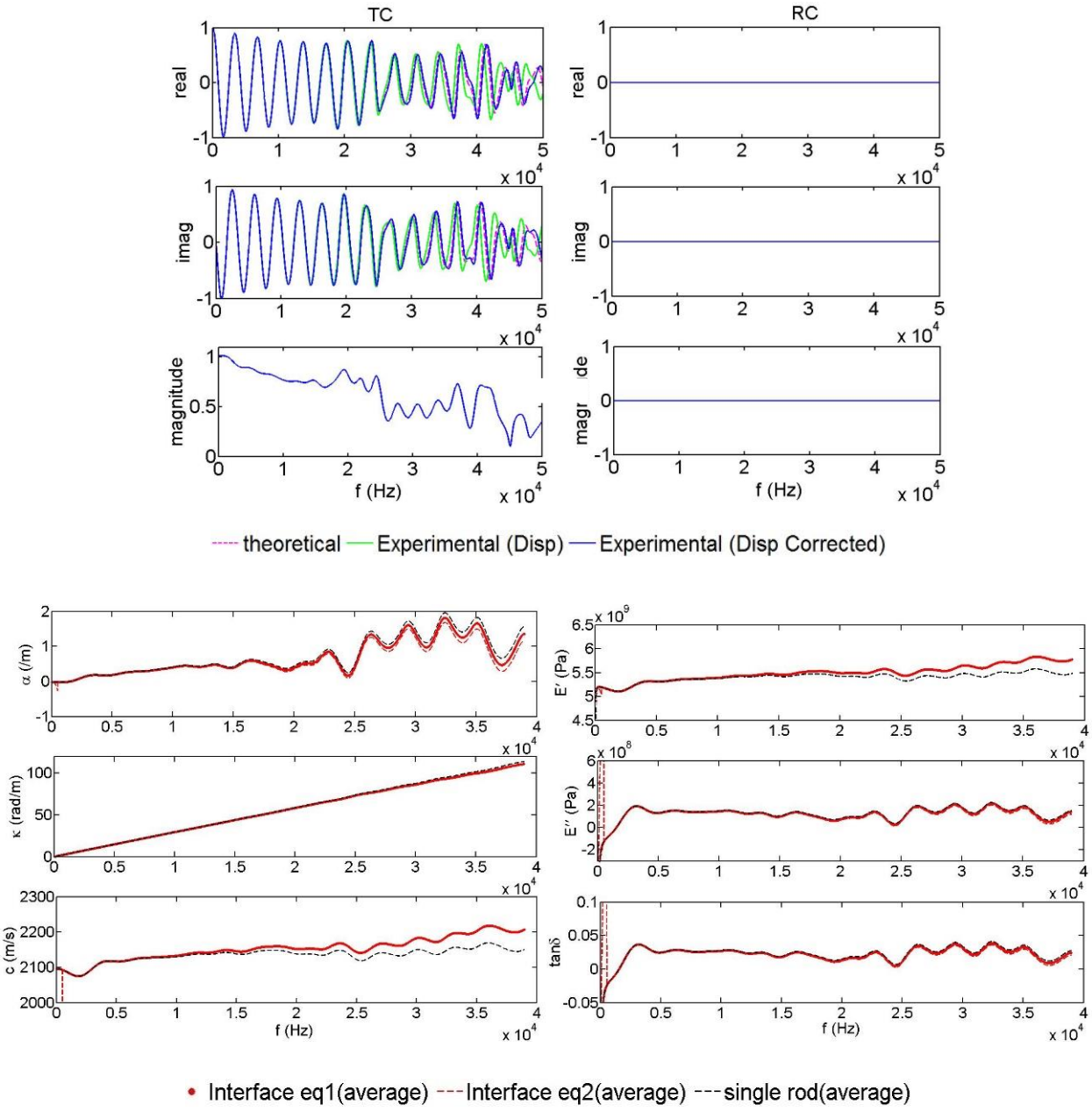

Figure 32. Top: Transmission and reflection coefficients and (Bottom) material properties derived from the data in Figure 31.

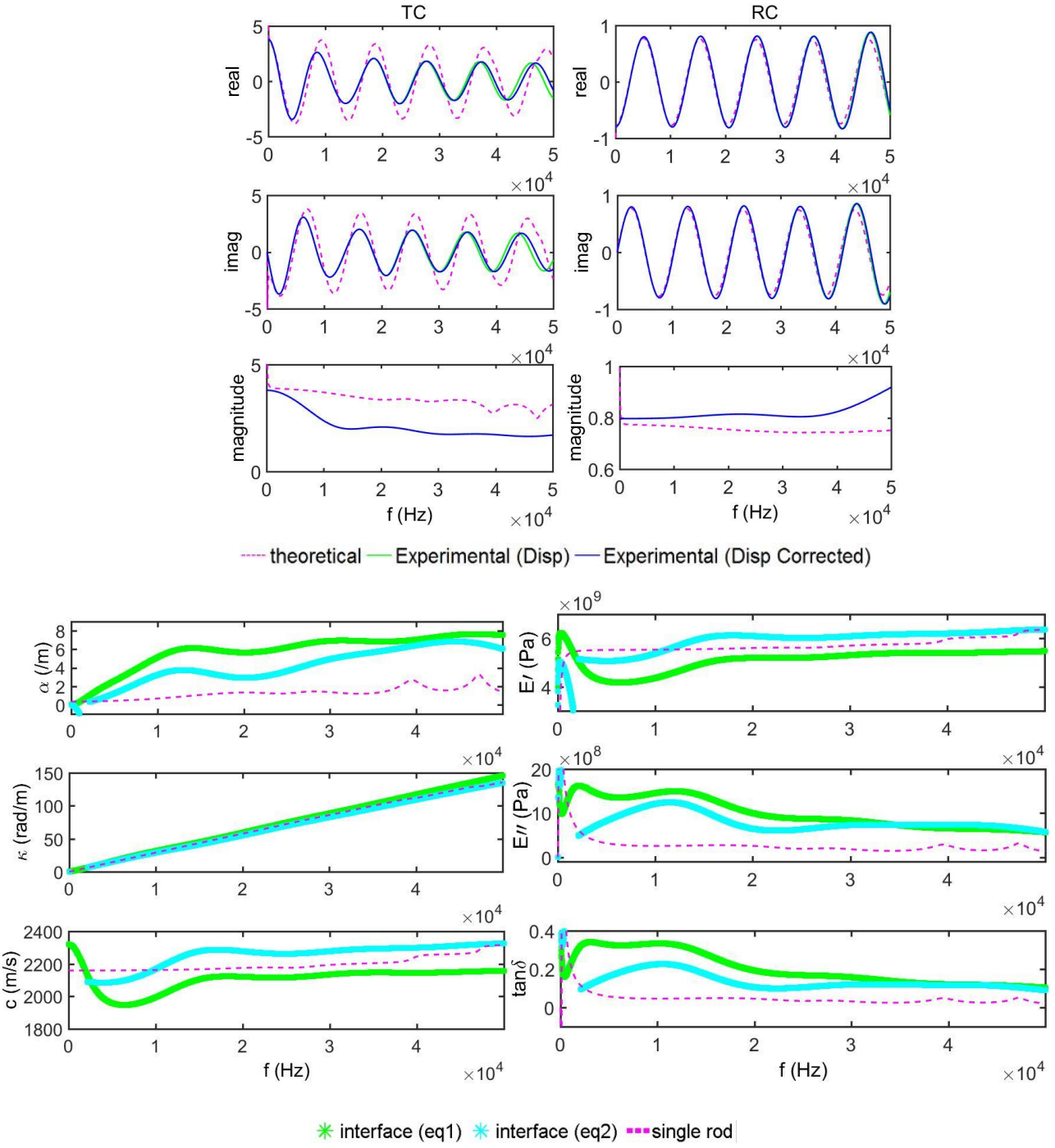

Figure 33. Top: Transmission and reflection coefficients; and Bottom: wave propagation parameters and PMMA modulus calculated from a Ti – PMMA interface.

4 Conclusions

A number of experimental techniques have been developed based on monitoring the propagation of stress waves in polymer specimens. In particular, the concept of incorporation of acceleration fields into the Virtual Fields Method, an idea that has been used by previous authors for linear elastic materials, has been utilised in a number of original experimental configurations to obtain rate, frequency and temperature dependence of elastomers under small and large deformations. It has been shown that monitoring stress wave propagation in slender rods of linear viscoelastic materials allows accurate determination off the frequency dependent complex modulus of these materials. In addition, an extensive theoretical framework for obtaining these properties from wave transmission and reflection coefficients has been developed. However, whilst experimental results are promising, further work is required to confidently apply these to obtain the properties of linear viscoelastic materials.

5 Acknowledgements

The authors would like to thank R Duffin, R Froud, N Warland and A Bateman for their technical support during this project. We also thank S Fuller, M Snyder, J Foley and J Jordan for both financial and intellectual support of the research.

6 References

1. Field, J.E., et al., *Review of experimental techniques for high rate deformation and shock studies.* International Journal of Impact Engineering, 2004. **30**(7): p. 725-775.
2. Siviour, C., *High Strain Rate Characterization of Polymers*, in *APS SCCM 2015*, R. Chau, T. Germann, and T. Swewell, Editors. 2015, American Physical Society: Tmpa, Florida.
3. Siviour, C.R. and J.L. Jordan, *High Strain Rate Mechanics of Polymers: A Review.* J. dynamic behavior mater., 2016. **2**: p. 15-32.
4. Moulart, R., et al., *Full-Field Strain Measurement and Identification of Composites Moduli at High Strain Rate with the Virtual Fields Method.* Experimental Mechanics, 2011. **51**(4): p. 509-536.
5. Pierron, F. and P. Forquin, *Ultra-High-Speed Full-Field Deformation Measurements on Concrete Spalling Specimens and Stiffness Identification with the Virtual Fields Method.* Strain, 2012. **48**(5): p. 388-405.
6. Pierron, F. and M. Grediac, *The Virtual Fields Method: Extracting Constitutive Mechanical Parameters From Full-field Deformation Measurements*. 2012. 1-517.
7. Pierron, F., M.A. Sutton, and V. Tiwari, *Ultra High Speed DIC and Virtual Fields Method Analysis of a Three Point Bending Impact Test on an Aluminium Bar.* Experimental Mechanics, 2011. **51**(4): p. 537-563.
8. Pierron, F., H. Zhu, and C. Siviour, *Beyond Hopkinson's bar.* Philosophical Transactions of the Royal Society a-Mathematical Physical and Engineering Sciences, 2014. **372**(2023).
9. Kolsky, H., *Stress Waves in Solids*. 1953, Oxford: Clarendon Press.